The Use of Fluorescence Methods to Monitor Unfolding Transitions in Proteins

Maurice R. Eftink
Department of Chemistry, University of Mississippi, University, Mississippi, USA

ABSTRACT This article discusses several strategies for the use steady-state and time-resolved fluorescence methods to monitor unfolding transitions in proteins. The assumptions and limitations of several methods are discussed. Simulations are presented to show that certain fluorescence observables directly track the population of states in an unfolding transition, whereas other observables skew the transition toward the dominant fluorescing species. Several examples are given, involving the unfolding of *Staphylococcal aureus* nuclease A, in which thermodynamic information is obtained for the temperature and denaturant induced transitions in this protein.

GLOSSARY

A_{nfi}	Arrhenius pre-exponential factor for nonradiative quenching of excited state
α_i	pre-exponential factor of intensity decay
C_i	spectral shape parameter
Δ_i	width of gaussian shape
ΔG°_{un}, ΔH°_{un}, ΔS°_{un}, and $\Delta C_{p,un}$	free energy change, enthalpy change, entropy change, and heat capacity change for unfolding reaction
$\Delta G^\circ_{un,o}$	free energy change for unfolding reaction at reference temperature
$E_{a,fi}$	activation energy for nonradiative quenching process i
exλ and emλ	excitation and emission wavelength in nanometers
$F_{i,ex\lambda em\lambda}$	steady-state fluorescence intensity of component i at excitation wavelength exλ and emission wavelength emλ
f_i	fractional steady state intensity of component i
Φ_i	fluorescence quantum yield of component i
K_{un}	unfolding equilibrium constant
k_f	rate constant for radiative decay
k_{nf}	temperature-dependent rate constant for nonradiative deactivation
k_{nfo}	temperature-independent rate constant for nonradiative dectivation
λ	wavelength in nanometers
m	denaturant concentration index
Q	partition function
S	general spectroscopic signal
s_N and s_U	baseline slopes of the native and unfolded states as a function of temperature or [denaturant]
$\sigma_{i,ex\lambda}$	absorption probability of component i at excitation wavelength exλ
ϕ_i	rotational correlation time of component i
r_i	steady-state anisotropy of component i
T	temperature
T_{un}	unfolding temperature, at which $\Delta G^\circ_{un} = 0$
T_o	reference temperature
τ_i	fluorescence decay time of component i
Θ_ω	phase angle at modulation frequency, ω
ν	frequency in cm^{-1} of center of gaussian shape function
v	thermal scanning rate in °C/s

INTRODUCTION

One of the practical uses of fluorescence techniques is to obtain thermodynamic and kinetic information about transitions of macromolecules, such as protein folding reactions. The sensitivity of fluorescence allows studies to be performed at micromolar (or lower) concentrations, which both minimizes the needed quantity of biomacromolecule and problems associated with aggregation and low solubilities. Also, fluorescence signals are usually very sensitive to the conformational state of a macromolecule. A limitation is that many fluorescence signal changes cannot be directly or unequivocally related to molecular details. However, thermodynamic (provided a transition is reversible) and kinetic information can usually be obtained from fluorescence studies.

With the availability of many mutant proteins, it is often of interest to study their folding mechanism and stability (Matthews, 1987; Oxender and Fox, 1987). The intent of this article is to consider the applications of and limitations of various fluorescence techniques to study transitions in proteins. Primarily, this article will focus on obtaining thermodynamic information for protein unfolding transitions.

In studies with proteins, the fluorophores can be either intrinsic (tryptophan, tyrosine residues, coenzyzmes) or extrinsic (attached dansyl, fluorescein, pyrene) probes. The fluorescence properties of various intrinsic and extrinsic probes will not be discussed here, but are covered in review articles (Beechem and Brand, 1985; Haugland, 1983; Eftink, 1991). Tryptophan residues are particularly valuable probes, since the indole ring is very sensitive to its environment and since there are often only a few tryptophan residues in a protein.

Received for publication 30 August 1993 and in final form 22 November 1993.

Address reprint requests to Dr. Maurice R. Eftink, Department of Chemistry, Coulter Hall, University of Mississippi, University, MS 38677.

0006-3495/94/02/482/20 $2.00

Below will first be discussed a general model for the unfolding of a protein, in order to provide a context for the discussion of the determination of thermodynamic data from fluorescence studies. Then will be presented the relationships between fluorescence signal changes and conformational transitions, the question of the uniqueness of the native and unfolded states, several practical considerations for fluorescence experiments, and the strategy of linking multiple data sets in the global analysis of data. Finally, several examples of the use of various fluorescence techniques to study protein folding reactions will be presented.

MATERIALS AND METHODS

Wild-type *Staphylococcal* nuclease A and the hybrid mutant, nuclease conA S28G, were obtained as described in Eftink et al. (1991a). The proteins were dissolved in 0.1 M NaCl, 0.01 M Tris-HCl, pH 7.0. Guanidine-HCl and urea were ultrapure grade from United States Biochemicals Inc.

Steady-state fluorescence measurements were made with a Perkin-Elmer MPF 44A, with a thermoregulated cell holder. Time-resolved fluorescence intensity decay data and anisotropy decay data were obtained with a phase/modulation fluorometer and were analyzed as described in Eftink et al. (1991a, *b*).

THERMODYNAMIC MODELS FOR THE UNFOLDING OF A PROTEIN

The unfolding of a monomeric protein may be described by the following two-state model, where N is the native state and U is the unfolded state of the protein, k_{un} and k_f are the rate constants (assuming a single step process) for the unfolding and refolding processes, K_{un} is the unfolding equilibrium constant, Q is the partition function, X_N and X_U are the mole fraction of protein molecules in the respective states, and ΔH°_{un} and ΔS°_{un} are the enthalpy change and entropy change for the unfolding transition.

$$N \underset{k_f}{\overset{k_{un}}{\rightleftharpoons}} U \tag{1}$$

$$K_{un} = [U]/[N] = k_{un}/k_f \tag{2}$$

$$Q = 1 + K_{un} \tag{3}$$

$$X_N = 1/Q; \qquad X_U = K_{un}/Q = 1 - X_N \tag{4}$$

$$\Delta G^\circ_{un} = -RT \cdot \ln K_{un} = \Delta H^\circ_{un} - T \cdot \Delta S^\circ_{un} \tag{5}$$

The N macroscopic state is considered to be an ensemble of molecules which share a common fold. It is assumed that the structure of a globular protein in solution is like that of the crystal structure. There may exist microscopic substates within N, but the microstates undergo the above N $\rightleftharpoons$ U transition in a similar manner (Lumry et al., 1966). The U macroscopic state is considered to be more or less a random coil, with little or no regular structure. As will be discussed below, there may exist some residual structure or compactness of the U state produced by certain denaturing conditions. Of concern in this article is how such microstates (of N or U) and residual structure (of U) affect fluorescence measurements and whether thermodynamic data for a transition can be unambiguously extracted from fluorescence data.

For thermally induced transitions, analysis of fluorescence data is intended to provide values of ΔH°_{un} and ΔS°_{un} (or the transition temperature, T_{un}, which equals $\Delta H^\circ_{un}/\Delta S^\circ_{un}$). For the unfolding of globular proteins, the ΔH°_{un} and ΔS°_{un} values are dependent on temperature (Privalov, 1989, 1990; Schellman, 1987). The temperature dependence of ΔH°_{un} is the heat capacity change, $\Delta C_{p,\,un}$, for the unfolding transition ($\Delta C_{p,\,un} = d\Delta H^\circ_{un}/dT$). Consequently, the free energy change for thermal unfolding is more correctly given by the following equation (rather than Eq. 5)

$$\Delta G^\circ_{un} = \Delta H^\circ_{o,\,un} + \Delta C_{p,\,un} \cdot (T - T_o) - T \cdot [\Delta S^\circ_{o,\,un} + \Delta C_{p,\,un} \ln(T/T_o)] \tag{6}$$

where $\Delta H^\circ_{o,\,un}$ and $\Delta S^\circ_{o,\,un}$ are the enthalpy change and entropy change for the unfolding reaction at some reference temperature, T_o (for example, this reference temperature may be chosen to be 0, 20°C or T_{un}). Since $\Delta C_{p,\,un}$ for the unfolding of globular proteins has positive values, Eq. 6 predicts that the stability of a protein (as measured by a positive ΔG°_{un}) goes through a maximum and that unfolding will occur at both a high temperature and at a low temperature (i.e., cold unfolding). See Privalov (1990), Schellman (1987), and Becktel and Schellman (1987) for further discussion of the thermodynamics of protein unfolding, with emphasis on the phenomenon of cold unfolding. In fluorescence studies with globular proteins, it is important to realize that cold unfolding is known to exist and some fluorescence data at low temperature may be sensitive to such transitions.

Besides thermally induced unfolding of proteins, a second way in which the unfolding of proteins is commonly induced is by the addition of a chemical denaturant, such as guanidine-HCl or urea. In these cases, the ΔG°_{un} is dependent on the concentration of denaturant, [D]. The following linear relationship is generally accepted to describe the thermodynamics of denaturant induced unfolding of proteins (Schellman, 1978; Pace, 1986).

$$\Delta G^\circ_{un} = \Delta G^\circ_{o,\,un} - m \cdot [D] \tag{7}$$

where $\Delta G^\circ_{o,\,un}$ is the free energy change for the unfolding reaction in the absence of denaturant at some reference temperature (usually selected to be 20 or 25°C) and m is a denaturant index (i.e., $m = -d\Delta G^\circ_{un}/d[D]$, the dependence of ΔG°_{un} on denaturant concentration).

The above discussion of protein unfolding has assumed that the process is a single step (two-state) process. If there is one or more intermediates in the unfolding process, then the thermodynamic models become more complex. Consider the unfolding reaction in which an intermediate state, I, is significantly populated

$$N \rightleftharpoons I \rightleftharpoons U \tag{8}$$

$$K_{N\to I} = [I]/[N]; \qquad K_{I\to U} = [U]/[I] \tag{9}$$

The corresponding $\Delta G^\circ_{N\to I}$, $\Delta H^\circ_{N\to I}$, $\Delta S^\circ_{N\to I}$, $\Delta G^\circ{}_{o,\,N\to I}$, $m_{N\to I}$, $\Delta G^\circ_{I\to U}$, $\Delta H^\circ_{I\to U}$, $\Delta S^\circ_{I\to U}$, $\Delta G^\circ_{o,\,I\to U}$, and $m_{I\to U}$ can be defined for the two step process. The partition coefficient and mole fraction of molecules in each macroscopic state are

given by

$$Q = 1 + K_{N\to I} + K_{N\to I} \cdot K_{I\to U} \quad (10)$$

$$X_N = \frac{1}{Q}; \quad X_I = \frac{K_{N\to I}}{Q}; \quad X_U = \frac{K_{N\to I} \cdot K_{I\to U}}{Q} \quad (11)$$

Identifying the existence of an intermediate, characterizing its spectral properties, and determining the thermodynamics of a three-state unfolding transition are difficult challenges. The ability to do this will depend on how extensively the intermediate state is populated and will require a significant difference in the fluorescence properties of the three states. If the fluorescence properties of the I and U states (or the N and I states) are similar, the transition may appear to be two-state.

FLUORESCENCE SIGNAL CHANGES AND CONFORMATIONAL TRANSITIONS

In order for any spectroscopic method to be used to monitor a conformational transition of a macromolecule, there must be a discernable difference in some signal between the two or more macroscopic states. Fluorescence spectroscopy is very useful for such studies because fluorescence signals are extremely sensitive to the microenvironment of a fluorophore. Fluorescence is an intrinsically multi-dimensional method and enables measurements to be made as a function of wavelength, time (i.e., decay time of the excited state or reaction time for a conformational transition), polarization angle, or solvent conditions (i.e., addition of quencher, D_2O, hydrogen ion, etc). The multi-dimensional character of fluorescence makes it likely that some signal will be sensitive to the conformational state of a macromolecule. Absorption and fluorescence transitions occur on the femtosecond and nanosecond time scales, respectively. Since macroscopic conformational changes in proteins occur on a much longer time scale, there will not be dynamic averaging of signals from the various macrostates. Also, fluorescence is a very convenient and adaptable method (light in, light out) for various sample chambers, types of preparations, or experimental designs. Finally, a broad range of protein concentration can be studied (nanomolar to millimolar), which can minimize the amount of sample needed and/or can enable protein-protein aggregation to be characterized or minimized.

Among the fluorescence signal changes that can be monitored are the following: fluorescence intensity (at some excitation and emission wavelengths, exλ and emλ), $F_{ex\lambda em\lambda}$; quantum yield, Φ; emission maximum, λ_{max}; fluorescence lifetime, τ_i, pre-exponential factor, α_i; fluorescence anisotropy, r; and rotational correlation time, ϕ. Each of these signals has been used by researchers to monitor protein unfolding transitions (Gryczynski et al., 1988; Eftink et al., 1991*a*, *b*; Mei et al., 1992). Critical to the use of any of these signals is whether the signal is proportional to the population of macrostates. That is, to be useful a fluorescence signal (here we use **S** to indicate some general signal) must be related to the mole fraction of molecules in macrostate i as follows

$$\mathbf{S} = \sum X_i \mathbf{S}_i \quad (12)$$

where $\mathbf{S}_i$ is the intrinsic (molar or relative) signal for a given macrostate, and X_i is the mole fraction of molecules in macrostate i and can be related to the thermodynamics of the transition by models and equations, such as Eqs. 1–5.

The most straightforward fluorescence signal that satisfies equation 12 is the fluorescence intensity, $F_{ex\lambda em\lambda}$, measured at some pair of excitation and emission wavelengths. Although a little more complicated, the apparent fluorescence quantum yield, Φ, and the pre-exponential factors, α_i, for a multi-exponential intensity decay also satisfy Eq. 12. Other fluorescence signals, including the emission anisotropy, r, and average fluorescence lifetime, $\bar{\tau}$ (see below the distinction between average and mean lifetimes), do not linearly track the mole fraction of macrostates, X_i, although several researchers have used these other signals to monitor protein unfolding. These latter signals are weighted by both the fraction of states and by the fluorescence quantum yield of each state, i.e. $\mathbf{S} = \sum \mathbf{S}_i X_i \Phi_i / \sum X_i \Phi_i$, and thus determination of thermodynamic parameters from these signals can yield inaccurate results. To illustrate how some signals track X_i and some do not, I present the following simulations.

Simulations

Consider the unfolding of a protein to be a two-state process. Further, consider the three cases in Fig. 1 (and Table 1) for the different fluorescence signals for the N and U states. In *Case I*, the unfolding of the protein results in a red shift from 330 nm to 350 nm, a decrease in the quantum yield and fluorescence decay time (assumed for simplicity to be monoexponential for both pure states), a decrease in the rotational correlation time of the fluorophore, and a slight blue shift in the absorbance spectrum of the U state. In *Case II*, the spectral changes are the same except that the decrease in quantum yield and decay time are greater. In *Case III* there is a very large enhancement in quantum yield and decay time upon unfolding; this may simulate a situation in which the unfolding of a protein relieves the quenching of a tryptophan residue by a heme group, as in the case of cytochrome c or myoglobin. In each case the simulated absorption and emission spectra are Gaussian in shape; the normalized spectral shape functions, C_i, are given by

$$C_{i,\nu} = \frac{\exp[(\nu_i - \nu)^2/\Delta_i^2]}{\Delta_i\sqrt{2\pi}} \quad (13)$$

where ν is wavenumber (= 1/wavelength in cm^{-1}), ν_i is the wavenumber for the center of the Gaussian curve, and Δ_i is the width of the curve in cm^{-1}. The shape functions were simulated in wavenumber, where the spectra should be symmetrical shapes, and then converted to the more familiar wavelength axis. Note that this shape function is normalized so that the $\sum C_{i,\nu} = 1.0$. In simulating an absorbance spectrum, a maximum molar extinction coefficient of 5×10^3 M^{-1} cm^{-1} was assumed for each state.

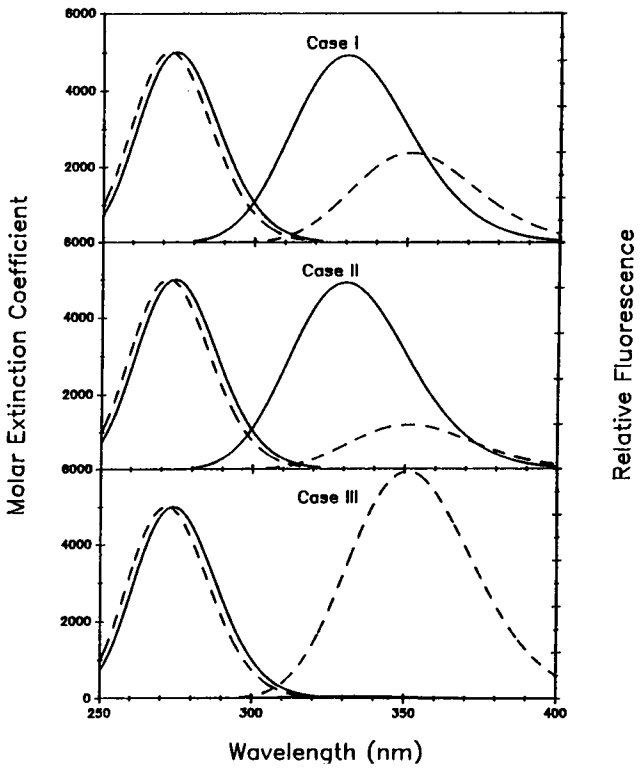

FIGURE 1 Simulated excitation and emission spectra for N state (——) and U state (– – –). *Case I:* $\Phi_N = 0.2$, $\Phi_U = 0.1$, $\lambda_{max} = 330$ nm for N state, $\lambda_{max} = 351$ nm for U state. *Case II:* $\Phi_N = 0.2$, $\Phi_U = 0.05$, $\lambda_{max} = 330$ nm for N state, $\lambda_{max} = 351$ nm for U state. *Case III:* $\Phi_N = 0.0025$, $\Phi_U = 0.25$, $\lambda_{max} = 330$ nm for N state, $\lambda_{max} = 351$ nm for U state. See Table 1 for other parameters used to simulate the spectra.

TABLE 1 Parameters for simulated spectra and fluorescence data

	Case I	Case II	Case III
Native state, N			
λ_{max} (nm)	330	330	330
ν (cm^{-1})	30.3	30.3	30.3
Δ (cm^{-1})	2.5	2.5	2.5
Φ	0.2	0.2	0.0025
τ (ns)	4.0	4.0	0.05
ϕ (ns)	10.0	10.0	10.0
r	0.143	0.143	0.199
Unfolded state, U			
λ_{max} (nm)	351	351	351
ν (cm^{-1})	28.5	28.5	28.5
Δ (cm^{-1})	2.3	2.3	2.3
Φ	0.1	0.05	0.25
τ (ns)	2.0	1.0	5.0
ϕ (ns)	1.0	1.0	1.0
r	0.0667	0.10	0.0333

For each case, $k_f = 5 \times 10^7$ s^{-1}. The simulated absorption spectra for each case were as follows: for the N state, $\nu_N = 36.5$ cm^{-1} (274 nm), $\Delta_N = 2.5$ cm^{-1}, and maximum $\epsilon_N = 5 \times 10^3$ M^{-1} cm^{-1}; for the U state, $\nu_U = 36.8$ cm^{-1} (272 nm), $\Delta_U = 2.5$ cm_{-1}, and maximum $\epsilon_U = 5 \times 10^3$ M^{-1} cm^{-1}. At 295 nm, the molar extinction coefficients are equal to 1693 M^{-1} cm^{-1} for the N state and 1300 M^- cm^{-1} for the U state. Wtih excitation at 295 nm, 56.56% of the light is absorbed by the N state. An isosbestic point is at 273 nm.

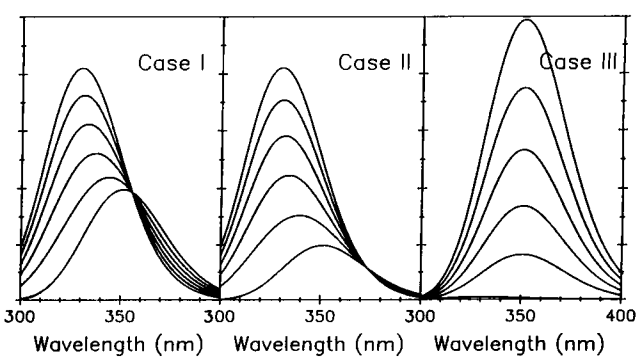

FIGURE 2 Simulated spectra for a mixture of N and U states. The series of curves in each panel are for $X_{un} = 0$, 0.2, 0.4, 0.6, 0.8, and 1.0.

Shown in Fig. 1 are the simulated absorbance spectra and emission spectra for the N and U states for these three cases. Using these simulated spectral shapes, and the assumed quantum yields, decay times, and rotational correlation times (see Table 1), data were simulated for transitions between the pure N and U states. Shown in Fig. 2 are emission spectra as X_U increases from 0 to 1.0. (Other spectral data were simulated using equations given below.) Shown in Fig. 3 are steady-state fluorescence intensity data (at a constant exλ and emλ), the apparent quantum yield, steady state anisotropy, and average fluorescence lifetime for the transition. Shown in Fig. 4 are results of the analysis in different ways of the intensity decay data (see below). (In all cases except the fluorescence intensity, the data shown are for the emission observed over the entire emission envelope).

To realistically relate the simulated fluorescence signal changes to a protein unfolding experiment, the X_U values were related to a denaturant (i.e., urea or guanidine-HCl) concentration, by combining equations 4 and 7. To simulate denaturant unfolding curves, we assumed $\Delta G^\circ_{o,un} = 5.0$ kcal/mol and $m = 1.5$ kcal·liter/mol^2, which are typical values for the unfolding of a globular protein, and we included a 1% random error in the various fluorescence signals. No baseline slopes (see below) were assumed in the simulations. Also, note that an exλ of 295 nm was assumed. The simulated N and U states have slightly different ϵ_{295}; the N state absorbs slightly more of the excitation light at this wavelength (i.e., for a 50:50 mixture of N and U states, the N state would absorb 56.56% of the light), so the fluorescence data in the transition range reflects differences in both the emission and excitation properties of the N and U states. The simulations are given in terms of an urea or guanidine induced unfolding transition, since the form of Eq. 7 is simple. However, the simulations could also apply to thermal (or pressure) induced unfolding transitions, by using Eqs. 5, 6, or 33.

The simulated data in Fig. 3 were then analyzed (by nonlinear least squares analysis with Eqs. 4 and 7 and an equation given below) to try to recover the assumed values of $\Delta G^\circ_{o,un}$, m and the fluorescence signals for the pure states. The data sets were fitted with the equations given below and the recovered parameters are given in Table 2 for the various types

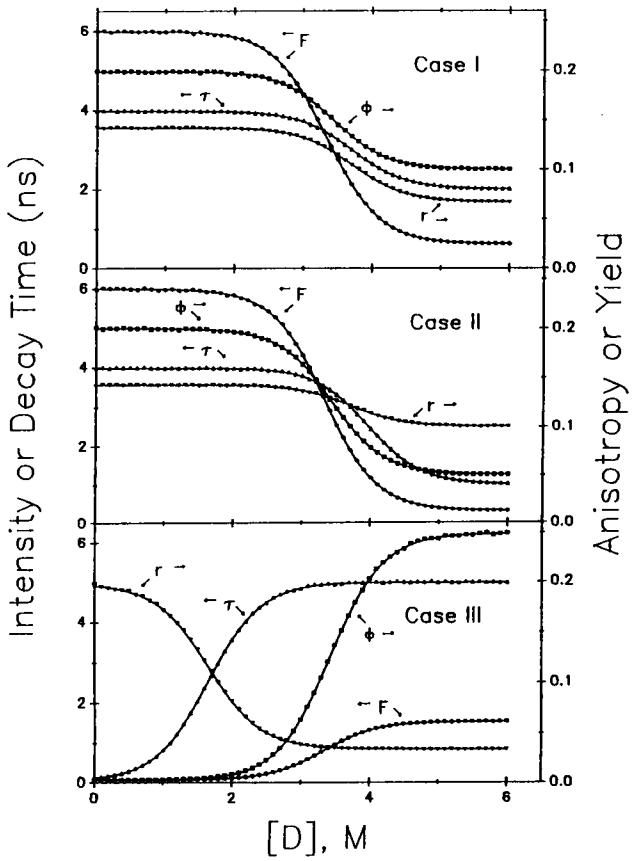

FIGURE 3 Simulated data for the denaturant induced unfolding of a protein. Shown for the three cases are profiles of the fluorescence intensity at 320 nm (●, *left axis*), the average lifetime, $\bar{\tau}$ (▲, *left axis*), the apparent quantum yield (■, *right axis*), and the steady-state anisotropy (▼, *right axis*). The solid curves are fits to Eqs. 4, 7, and 12′ with the parameters given in Table 2. "Data" were simulated to have 1% random error, and the baseline regions were assumed to have zero slope.

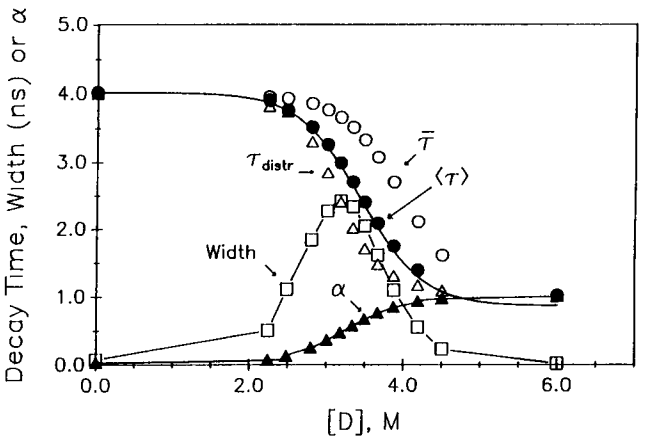

FIGURE 4 Simulated fluorescence lifetime data for the denaturant induced unfolding of a protein. Shown are the average decay time, $\bar{\tau}$ (○), the mean decay time, $\langle\tau\rangle$ (●), the unimodal Lorentzian distribution lifetime (△) and distribution width (□), and the pre-exponential factor, α_U (▲), for the short decay time. The curve shown through the mean decay time and pre-exponential factor "data" are for the fitting parameters given in Table 2.

of fluorescence data and for the three cases listed above. Below I will give equations describing each type of spectral data and comment on how well the thermodynamic parameters can be recovered from each type of data. In the fittings, it was assumed that there can exist pre- and post-transition baseline slopes for the $\mathbf{S}_i$ for each state, i.e., it was assumed that

$$\mathbf{S}_i = \mathbf{S}_{io} + \mathbf{S}_i[\mathrm{D}] \qquad (12')$$

where $s_i = d\mathbf{S}_i/d[\mathrm{D}]$ is the baseline slope for $\mathbf{S}_i$ versus [D]. Allowing for the existence of a slope for the fluorescence signal of each state as a function of perturbant makes the nonlinear least-squares fits more realistic (see Eqs. 23 and 25 for the full form of an equation that includes baseline slopes).

The *fluorescence intensity* is related to the mole fraction of states by

$$F_{ex\lambda em\lambda} = \sum X_i \sigma_{i,\,ex\lambda} F_{i,\,em\lambda} / \sum X_i \sigma_{i,\,ex\lambda} \qquad (14a)$$

$$F_{ex\lambda em\lambda} \approx \sum X_i F_{i,\,em\lambda} \qquad (14b)$$

where $F_{i,\,em\lambda} = C_{i,\,em\lambda}\Phi_i$ is the fluorescence intensity of state i at emission wavelength emλ and $\sigma_{i,\,ex\lambda}$ is the fractional absorption coefficient of state i at exλ (i.e., $\sigma_{N,\,ex\lambda} = \epsilon_{N,\,ex\lambda}/(\epsilon_{N,\,ex\lambda} + \epsilon_{U,\,ex\lambda})$, where ϵ are molar extinction coefficients; with exλ = 295 nm, $\sigma_{N,\,295} = 0.5656$ for the simulation). If the $\sigma_{i,\,ex\lambda}$ are the same for each species (i.e., an isosbestic excitation wavelength), then Eq. 14a simplifies to $F_{ex\lambda em\lambda} = \sum X_i F_{i,\,em\lambda}$ and X_i can be readily determined from data. As long as $\sigma_{N,\,ex\lambda} \approx \sigma_{U,\,ex\lambda}$, Eq. 14b (which is of the form of Eq. 12) is a good approximation.

The fits through the simulated intensity versus [D] data in Fig. 3 (with six fitting parameters, $F_{N,\,em\lambda}$, $F_{U,\,em\lambda}$, s_N, s_U, $\Delta G^\circ_{o,\,un}$, and m; see listings in Table 2) show a good recovery of the $\Delta G^\circ_{o,\,un}$ and m values for all three cases when the intensity is observed either at the blue (320 nm) or red (360 nm) side of the emission band. The recovered $\Delta G^\circ_{o,\,un}$ and m values are only 1–3% and 1–8% larger, respectively, than the inputted values of $\Delta G^\circ_{o,\,un}$ = 5.0 kcal/mol and m = 1.5 kcal·liter/mol^2. This slight difference can be attributed to the 1% random error introduced in the simulation and to the fact that $\sigma_{N,\,ex\lambda}$ is slightly greater than $\sigma_{U,\,ex\lambda}$, which results in more excitation into the N state and a slight overestimation of X_N and $\Delta G^\circ_{o,\,un}$ (when Eq. 14b is used).

The apparent *quantum yield* is given by

$$\Phi_{app} = \sum X_i \sigma_{i,\,ex\lambda} \Phi_i / \sum X_i \sigma_{i,\,ex\lambda} \qquad (15a)$$

$$\Phi_{app} \approx \sum X_i \Phi_i \qquad (15b)$$

where Φ_i is the quantum yield of state i. Again, if $\sigma_{N,\,ex\lambda} \approx \sigma_{U,\,ex\lambda}$, then Eq. 15b can be used; it is of the form of Eq. 12. Analysis of Φ_{app} versus [D] data with Eqs. 4, 7, and 15b yields fits with $\Delta G^\circ_{o,\,un}$ and m values that are only ~5% and ~2% larger that the inputted values (see Table 2). Thus both intensity and apparent quantum yield measurements track the N to U transition.

TABLE 2 Analysis of simulated data in terms of a two-state transition (assumed $\Delta G^0_{o,un}$ = 5.0 kcal/mol and m = 1.5 kcal·liter/mol²)*

	$\Delta G^0_{o,un}$ (kcal/mol)	m_{un} (kcal·liter/mol²)	S_N	S_U
Case I				
Intensity (320)	5.064	1.518	5.982	0.582
Intensity (360)	5.089	1.626	2.495	0.609
Quantum Yield	5.230	1.521	0.1999	0.098
Anisotropy	5.683	1.534	0.1423	0.0668
Average τ	5.706	1.542	3.979	2.036
Mean τ	5.293	1.541	3.976	2.036
Pre-exponential	5.469	1.628	0.963	0.048
Average ϕ	5.661	1.529	9.947	1.037
Emission λ_{max}	6.630	1.768	330.0	357.2
Case II				
Intensity (320)	5.135	1.540	5.991	0.351
Intensity (360)	5.076	1.521	2.499	1.152
Quantum Yield	5.276	1.535	0.1992	0.0505
Anisotropy	5.610	1.510	0.1422	0.0980
Average τ	6.041	1.524	3.972	1.038
Mean τ	5.290	1.540	3.983	1.024
Pre-exponential	5.214	1.608	0.989	0.022
Average ϕ	6.001	1.511	9.945	0.872
Emission λ_{max}	7.729	1.914	330.1	354.5
Case III				
Intensity (320)	5.045	1.518	0.748	1.514
Intensity (360)	5.069	1.521	0.313	5.765
Quantum Yield	5.271	1.536	0.00242	0.2458
Anisotropy	2.551	1.535	0.1979	0.0333
Average τ	2.517	1.519	0.0487	5.000
Mean τ	5.236	1.525	0.0498	4.984
Pre-exponential	4.915	1.521	1.000	0.0002
Average ϕ	2.520	1.524	9.965	0.994
Emission λ_{max}	3.551	2.173	329.9	349.5

* The table lists fitting parameters obtained from nonlinear least-squares fits to simulated data. The slopes of pre- and post-translational baselines were also included as fittings parameters. The resulting slopes are not included in the table, but all are similar to the assumed values of s_N and s_U = 0.

The *steady-state anisotropy* is given by the following equation, in which the anisotropy for each state, r_i, is weighted by the quantum yield of each state.

$$r_{ex\lambda} = \frac{\sum X_i \sigma_{i,ex\lambda} \Phi_i r_i}{\sum X_i \sigma_{i,ex\lambda} \Phi_i} \qquad (16a)$$

$$r_{ex\lambda} \approx \frac{\sum X_i \Phi_i r_i}{\sum X_i \Phi_i} \qquad (16b)$$

This function differs in form from equation 12 and the experimental r values does not directly track the fraction of molecules in each state (actually, $r_{ex\lambda}$ is directly related to the fractional fluorescence intensity, $X_i\Phi_i/\sum X_i\Phi_i$, for each state). If $r_{ex\lambda}$ versus [D] data are analyzed by an equation having the form of Eq. 12, then a good fit can be obtained (see Fig. 3), but the recovered $\Delta G^\circ_{o,un}$ values overestimate the true value by 13% for Cases I and II and underestimate the true value by 50% for Case III (3.88 versus 5.0 kcal/mol, which is a significant difference). The recovered *m* values, in contrast, are within a few percent of the true value. Because the apparent anisotropy is skewed toward the state with the higher fluorescence quantum yield, the recovered $G^\circ_{o,un}$ values will also be skewed toward the more intensely emitting state. An analysis using the "correct" Eq. 16b should work, but this would involve two additional parameters (Φ_N and Φ_U), which may or may not be known quantities. The point is that steady-state anisotropy does not directly track the population of states and caution must be exercised in trying to obtain thermodynamic information from such measurements.

As with steady-state anisotropy, the fluorescence λ_{max}, average fluorescence lifetime, and average rotational correlation time also can give a skewed tracking of the population of states. The fluorescence λ_{max} will track the population of states only if the quantum yield (and the emission spectral width and absorbance) of the states is the same (and, of course, the λ_{max} for the two states differ). If one state has a higher quantum yield that the other, then the former will dominate the emission spectrum and the apparent λ_{max} will be skewed toward this state. There is no simple equation to describe the λ_{max} for a mixture of states (which have overlapping emission spectra), but I have simulated spectra as a function of [D] for Cases I, II, and III and have graphically determined the apparent λ_{max}. Fig. 5 shows the resulting plots along with fits to a function of the form of Eq. 12 (see Table 2). The recovered thermodynamic parameters are skewed, as expected; an extreme case is given by Case III. A more quantitative way to analyze the emission spectrum of a mixture is to fit the spectrum to the sum of individual spectra for the N and U states.

The fluorescence decay of a protein will become more heterogeneous (i.e., more nonexponential; unless $\tau_N = \tau_U$) in the transition region; there will be decay components with decay times τ_i for the pure N and U states. If time-resolved data are collected, the amplitude associated with each species can be directly monitored. Alternatively, the *average decay time*, $\bar{\tau}$, is defined as (for observation over

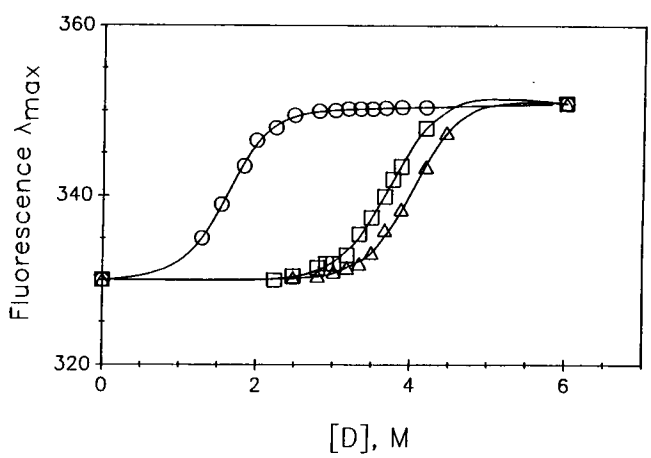

FIGURE 5 Simulated fluorescence λ_{max} as a function of [D] for Case I (□), Case II (△), and Case III (○). The curves through the "data" are for the fitting parameters given in Table 2.

the entire emission spectrum)

$$\bar{\tau} = \frac{\sum X_i \sigma_{i,\,ex\lambda} \Phi_i \tau_i}{\sum X_i \sigma_{i,\,ex\lambda} \Phi_i} \tag{17a}$$

$$\bar{\tau} \approx \frac{\sum X_i \Phi_i \tau_i}{\sum X_i \Phi_i} \tag{17b}$$

i.e., the individual decay times are weighted by both the population of states and the quantum yield of the states. As shown in Fig. 4 and Table 2, analysis of average decay time data in terms of Eq. 12 results in an inaccurate value of the thermodynamic parameters, with recovered $\Delta G^\circ_{o,\,un}$ values being up to 20% larger (Case II) or 20% smaller (Case III) than the true value. Again, the m values are still within 2–3% of the expected values. The average decay time, as defined above, will be approximately equal to the apparent mono-exponential decay for a mixture of N and U states (i.e., if a mono-exponential decay law, discrete or distributed, is used to fit data, even though the data are nonexponential). On the other hand, the *mean decay time*, $\langle\tau\rangle$, does track the population of states. $\langle\tau\rangle$ is defined as

$$\langle\tau\rangle = \frac{\sum X_i \sigma_{i,\,ex\lambda} \tau_i}{\sum X_i \sigma_{i,\,ex\lambda}} \tag{18}$$

which can be rewritten as $\langle\tau\rangle = \sum \alpha_i \tau_i$, where $\alpha_i = X_i \sigma_{i,\,ex\lambda} / \sum X_i \sigma_{i,\,ex\lambda}$ and is the pre-exponential pactor for a multi-exponential decay law. If the absorption coefficient, $\sigma_{i,\,ex\lambda}$, is the same for both N and U states, then $\alpha_i = X_i$. As shown in Fig. 4 and Table 2, the mean decay time can be used to track the population of states and to determine thermodynamic parameters. However, it must be remembered that it is $\bar{\tau}$, not $\langle\tau\rangle$, that is approximated by fitting nonexponential data to a single exponential (or unimodal distributed) decay law.

When such fluorescence decay data are analyzed in terms of a unimodal distributed decay law (Alcala et al., 1987*a*, *b*), the distribution (i.e, Lorentzian or Gaussian shape) becomes wider in the transition region. Fig. 4 shows this effect. While such an increase in width can indicate the existence of multiple states, it is not obvious how thermodynamic data can be quantitatively determined from such widths, since the widths depend on the disparity of the τ_i.

Likewise, the *anisotropy decay* of a protein will become more heterogeneous in the transition region. However, there should still exist components with rotational correlation times ϕ_i for the pure states. Anisotropy decay data are ususally described by the empirical equation, $r(t) = r_o \sum g_i \exp(t/\phi_i)$, where r_o is the anisotropy in the absence of motion and g_i is a pre-exponential term for each rotating mode. For a mixture of species, such as exists in a N $\rightleftharpoons$ U equilibrium, the anisotropy decay is more correctly described by (Knutson et al., 1986; Steiner, 1991)

$$r(t) = \frac{\sum X_i \sigma_{i,\,ex\lambda} r_o e^{-t/\tau_i} e^{-t/\Phi_i}}{\sum X_i \sigma_{i,\,ex\lambda} e^{-t/\tau_i}} \tag{19}$$

where the rotational correlation time of each species is "associated" with its intensity decay time. Thus $r(t)$ data possess information about X_i, but extraction of the latter will be with some difficulty. The situation is further complicated by the fact that the anisotropy decay of the native state of a protein is usually comprised of a ϕ_i for global tumbling of the macromolecule and a ϕ_i for segmental motion of the fluorophore. This latter, rapid motion may be on a similar time scale and thus difficult to distinguish from motion of the fluorophore in the unfolded state. (Later I will give an example of an attempt to analyze $r(t)$ data with the above equation.)

Another fluorescence signal that can be used to monitor a conformational transition is the *degree of energy transfer* between an attached donor, D, and an acceptor, A, on a protein. The DA distance may be characteristically different for the N and U states. The DA distance may be either larger or smaller in the U state, depending on the position of attachment of the D and A groups on the linear chain. If the U state is a random coil, then the distribution of DA distances is expected to be wider in the U state than in the N state. With an equilibrium mixture of states, the apparent degree of energy transfer, $E_{T,\,app}$ (where quenching of the donor by an acceptor is measured over the entire emission spectrum), is described by the following equation.

$$E_{T,\,app} = 1 - \frac{\sum X_i \sigma_{i,\,ex\lambda} \Phi_i (1 - E_{T,\,i})}{\sum X_i \sigma_{i,\,ex\lambda} \Phi_i} \tag{20a}$$

$$E_{T,\,app} \approx 1 - \sum X_i \sigma_{i,\,ex\lambda} \Phi_i (1 - E_{T,\,i}) \tag{20b}$$

where $E_{T,\,i}$ is the degree of energy transfer in state i between donor and acceptor and Φ_i is the quantum yield in the absence of donor. Thus, the determination of $E_{T,\,app}$ versus perturbation is weighted by the fluorescence intensity of the state and thus does not directly track the population of states.

Baseline trends

The above considerations and the fits in Fig. 3 argue that fluorescence intensity, quantum yield, intensity decay preexponentials, and the mean $\langle\tau\rangle$ are directly related to the population of macrostates for an N $\rightleftharpoons$ U transition and are recommended for studies of the thermodynamics and kinetics of protein unfolding reactions. The simulations that generated the "data" in Fig. 3 did not include the possibility that the fluorescence signal of a pure state can show a baseline trend with increasing denaturant, or increasing temperature, change in pH, etc. (Actually the simulations assumed baseline slopes of zero.) The nonlinear least-squares analysis did include the possibility of nonzero pre- and post-transition slopes (Eq. 12′) in order to be more realistic. If these baseline trends are large, it may make difficult the analysis of data to obtain thermodynamic information.

A frequently employed way to handle such data is to draw linear baseline regions and to then subtract these baselines from the signals in the transition range. This obviously can introduce some human error in drawing the slopes or in selecting which points to include in the baseline. A better approach is to use nonlinear regression to fit the entire body of

data, including terms for the baseline regions, as we have done in fitting the above analysis of simulated "data" (also see Eqs. 23 and 25 below). However, it is still necessary to assume a functional dependence of the baseline trend on the denaturing condition. It seems to always be assumed that the baseline trends are linear. Here we examine the validity of this assumption. We will also consider how extensive the data in the baseline regions must be in order to enable accurate thermodynamic parameters to be recovered.

It is well known that the quantum yield and fluorescence decay time of indole and its derivatives, such as *N*-acetyl-L-tryptophanamide (NATA), do not have an exactly linear dependence on temperature. The temperature dependence of the quantum yield of indole and NATA is described by the relationship (Kirby and Steiner, 1970)

$$\Phi = \frac{k_f}{k_f + k_{nfo} + \sum A_{nfi} \cdot \exp(-E_{a,nfi}/RT)} \qquad (21)$$

where k_f is the rate constant for radiative decay (assumed to be temperature independent), k_{nfo} is the rate constant for temperature-independent nonradiative processes (i.e., intersystem crossing to the triplet state), and A_{nfi} and $E_{a,nif}$ are the Arrhenius factor and activation energy for nonradiative process k_{nfi}. While the temperature dependence of Φ of indoles in aqueous solution is not exactly linear (Kirby and Steiner, 1970), within any 30°C temperature range, a plot of Φ versus temperature will appear to be nearly linear. In nonpolar solvents the temperature dependence of Φ of indoles is smaller, than in water, thus making the plots appear to be even more linear. The temperature dependence of the quantum yield or fluorescence intensity of globular proteins is generally found to be approximately linear. So the assumption of linear pre- and post-transition baselines is an accepted practice which should only be questioned when data over an extensive temperature range are available. The assumption of linearity requires two fitting parameters. To describe the Φ (or F) baselines by Eq. 21 would require a minimum of three fitting parameters (these being the ratios k_{nfo}/k_f, A_{nf}/k_f, and E_a, assuming only one significant temperature dependent nonradiative rate process). The fluorescence lifetime of NATA or other fluorophore is also described by an equation analogous to Eq. 21 (divide through by k_f to get an expression for τ). Again, the assumption of a linear baseline dependence of τ on temperature is usually acceptable.

To examine the limitations of the assumption of linear baselines, we show in Fig. 6 simulated intensity data for the temperature induced unfolding of a protein in which the two baseline regions are described by equation 21 (with $E_{a,nfi}$ = 3 kcal/mol for the N state and $E_{a,nfi}$ = 8 kcal/mol for the U state). The simulated data were analyzed with a combination of Eqs. 4, 5, and 14b (which is Eq. 23) and the assumption of linear baseline regions. Nonlinear least-squares analysis recovers the inputted thermodynamic parameters, ΔH°_{un} and ΔS°_{un}, within 5%.

Other commonly used denaturing reactions are to add urea or guanidine-HCl to proteins. Shown in Fig. 7 is the dependence of the fluorescence intensity (excitation at 295 nm, emission at 350 nm), quantum yield, and lifetime of NATA on the concentration of urea and guanidine-HCl. As previously reported by Schmid (1989) for tryptophan, for both denaturants the fluorescence signal of NATA increases with

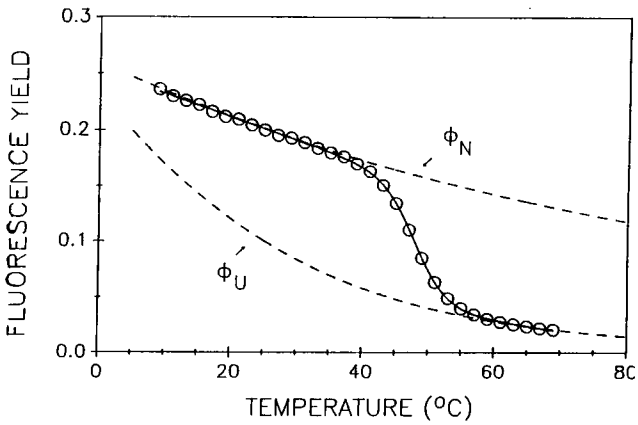

FIGURE 6 The effect of nonlinear baselines on the analysis of data for the thermally induced unfolding of a protein. The baselines were simulated using Eq. 21 with the assumption that the activation energy for the N and U states are 3.0 and 8.0 kcal/mol, respectively, and that the Arrhenius factors are 2.4×10^{10} and 3.1×10^{14} for the N and U states, respectively (with $k_f = k_{nfo} = 5 \times 10^7$ s^{-1} for both states). These values give the curved baselines for the pure states (shown as dashed lines). The transition was simulated with ΔH°_{un} = 80 kcal/mol, ΔS°_{un} = 250 cal/mol·deg (T_{un} = 47°C), and $\Delta C_{p,un}$ = 0. The simulated "data" were analyzed by assuming linear baselines, as discussed in the text, yielding ΔH°_{un} = 83.3 ± 2.0 kcal/mol and ΔS°_{un} = 259.4 ± 6.2 cal/mol·deg (T_{un} = 48.1°C).

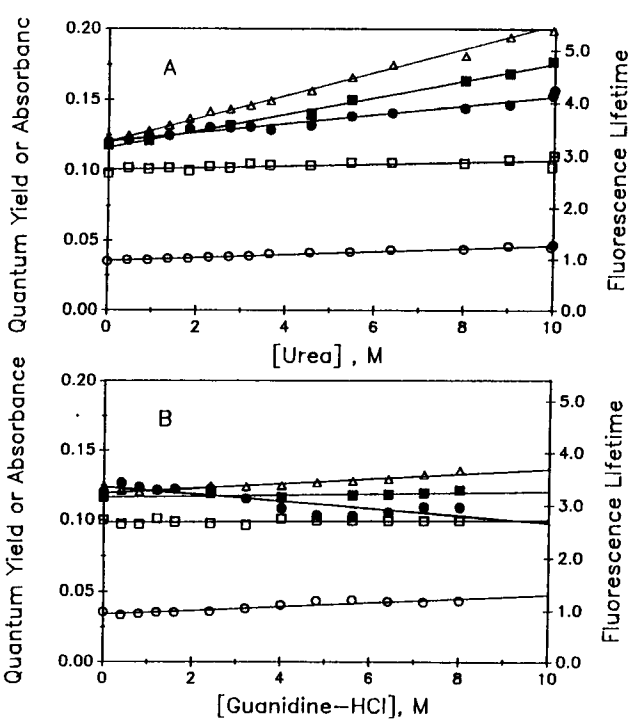

FIGURE 7 Dependence of the relative fluorescence intensity (△), absorbance at 280 nm (□) and 295 nm (○), fluorescence quantum yield (●), and mean fluorescence lifetime (■) of *N*-acetyl-L-tryptophanamide on the concentration of urea (*A*) and guanidine-HCl (*B*). Conditions: 20°C, pH 7.0.

added denaturant, with greater slopes being found with the addition of urea. The positive slopes of intensity versus [denaturant] can partially be explained by the increase in absorbance at 295 nm at higher [denaturant] (by comparison, the absorbance at 280 nm is virtually constant). Considering the effects of denaturant on both the fluorescence intensity and absorbance at 295 nm, the relative fluorescence quantum yield was calculated and shows a linear increase with [urea] and a small decrease with [guanidine-HCl]. The mean fluorescence lifetime of NATA also increases with [urea], to a degree that is slightly greater than the quantum yield. The lifetime of NATA is almost independent of [guanidine-HCl]. An explanation of these trends will not be attempted, but the patterns should be appreciated in the context of using these denaturants to induce changes in the fluorescence of proteins. The slopes in Fig. 7 are 0.069%/M for the relative intensity (295 excitation), 0.027%/M for the quantum yield, and 0.052%/M for the lifetime for NATA with urea as perturbant (slopes expressed as percentage of initial signal). The slopes are 0.015%/M for the relative intensity (295 excitation), −0.021%/M for the quantum yield, and <0.004%/M for the lifetime with guanidine-HCl as perturbant. Note that contaminant absorbance and fluorescence signals from the urea and guanidine were subtracted (actually they were negligible), so that the effects shown in Fig. 7 are real changes. The observation of nearly linear plots justifies the common practice of assuming linear baseline trends for urea and guanidine-HCl induced unfolding transitions, as monitored by fluorescence spectroscopy. The above slopes are expected to be similar to the values for a solvent exposed tryptophan residue, such as that in an unfolded protein. For an internal tryptophan residue the slopes are expected to be smaller.

A related and important question is how extensive must the baseline regions be in order to accurately recover thermodynamic parameters? Also, how necessary is it to have the protein fully folded in the initial part of the data (low [D] or low T)? To test this we simulated data for D induced unfolding in which the protein is only 89% folded at [D] = 0 ($\Delta G^\circ_{o,un}$ = 1.2 kcal/mol and m = 1.5 kcal·liter/mol^2) (see Fig. 8). These thermodynamic parameters pertain to a relatively unstable protein. We then analyzed data sets that were truncated, i.e., over the ranges of 0–6 M, 0–3 M, 0–2 M, 0–1.5 M, and 0–1 M. We first performed nonlinear least-squares fitting of Eqs. 4, 7, and 14b (which is Eq. 25 below) with the assumption that all fluorescence parameters, F_N, F_U, s_N, and s_U can vary. As shown in Table 3, the fits were able to recover the thermodynamic parameters with good accuracy (within ±10%), even when truncated to a data range of 0–1 M of denaturant. The SD of the recovered $\Delta G^\circ_{o,un}$ and m values becomes very large for the most truncated data set, but are acceptable for the other sets. (Of course, this success is partially due to the fact that only 1% random error was introduced into the simulated data; with higher random error, the success would be decreased.) However, the recovered fluorescence parameters are much less accurate and are unrealistic for the more truncated data, with negative fluorescence intensities and large slopes being obtained (even

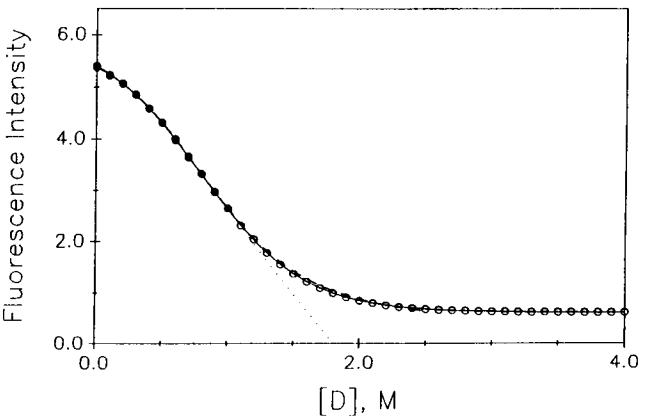

FIGURE 8 Effect of data range on the analysis of unfolding data. The unfolding of the protein was simulated with $\Delta G^\circ_{o,un}$ = 1200 cal/mol·deg and m = 1500 cal·liter/mol^2, making it marginally stable and having X_U = 0.11 at [D] = 0. The data over ranges 0–6, 0–3, 0–2, 0–1.5, and 0–1.0 M were analyzed (see Table 3). The open symbols are the actual curve used in the simulation. The solid symbols are data for the range 0–1.0 M. The dashed curve is a fit to the latter data range. The dotted curve is a fit in which the initial fluorescence signal is taken as being equal to $F_{N,o}$.

though slopes of zero were used to simulate the data). Since Fig. 7 shows that the slopes of the fluorescence of NATA as a function of [urea] and [guanidine] are small and positive values, we then analyzed the truncated data sets in Fig. 8 with assumed and fixed values of the slopes. That is, we fixed s_N = s_U = 0.05. With this assumption, the accuracy and precision of the recovered thermodynamic parameters is improved and the recovered F_N and F_U values are reasonable (results not shown in Table 3). This ploy of using assumed, fixed s_N and s_U values, for data such as that in Fig. 8, should be considered in actual cases in which the span of data is limited and baseline regions are ill defined.

Finally, we analyzed data by assuming that the initial fluorescence signal at [D] = 0 is equal to F_N and that s_N = 0. This is an assumption that is obviously incorrect, since the protein is only 89% folded at [D] = 0, but this is an assumption that is tempting to make. This is also an assumption that would be made if a researcher were not using nonlinear least squares to fit the data. As shown in Table 3, this faulty assumption leads to recovered $\Delta G^\circ_{o,un}$ values that are either too large (for the 0–6, 0–3, and 0–2 M data sets) or too small (the 0–1 M data set). In the latter case the recovered $\Delta G^\circ_{o,un}$ is as low as 0.35 kcal/mol (true value of 1.2 kcal/mol). The recovered m values are always overestimated, being off as much as 70%. Clearly, the latter assumption, that the initital signal is F_N, leads to inaccurate thermodynamic parameters in cases where the protein is not ~100% folded at [D] = 0 and this assumption should be avoided by using nonlinear least squares with F_N as a fitted parameter.

Basis for fluorescence signal changes

It is not necessary to fully understand the photophysical basis for the signal changes between the N and U state discussed

TABLE 3 Effect of limited data range on recovered thermodynamic parameters (for N ⇌ U with $\Delta G^0_{un,0}$ = 1200 cal/mol and m_{un} = 1500 cal/mol²

[D] range	$\Delta G^0_{0,un}$	m	F_N	F_U	s_N	s_U
0–6 M	1216	1519	6.004	0.610	−.0031	.065
	(18)	(53)	(.017)	(.004)	(.0005)	(.0009)
	1646	1845	⟨5.39⟩	0.723	⟨0⟩	−0.023
	(298)	(35)		(.035)		(.008)
0–3 M	1194	1535	5.995	0.611	0.210	0.109
	(33)	(15)	(.036)	(.33)	(.0001)	(.011)
	1704	2037	⟨5.37⟩	1.274	⟨0⟩	−0.236
	(41)	(65)		(.138)		(.055)
0–2 M	1142	1489	6.084	0.388	0.390	0.0952
	(82)	(63)	(.136)	(.298)	(.293)	(.125)
	1611	2311	⟨5.37⟩	2.685	⟨0⟩	−0.967
	(56)	(143)		(.296)		(.159)
0–1.5 M	1089	1415	6.245	−0.213	0.654	0.372
	(169)	(236)	(.575)	(2.22)	(.913)	(1.03)
	1118	2575	⟨5.37⟩	4.664	⟨0⟩	−2.266
	(124)	(143)		(.245)		(.664)
0–1.0 M	1190	1510	6.05	−0.64	0.505	0.725
	(330)	(460)	(.63)	(2.40)	(.786)	(1.38)
	354	1729	⟨5.37⟩	5.339	⟨0⟩	−2.984
	(59)	(136)		(.288)		(0.06)

Values in parentheses are the SD for the fitted parameters. Values in angle brackets, ⟨ ⟩, are fixed in the analysis.

above, in order to extract thermodynamic (or kinetic) information. However, some understanding of the basis for the signal changes can help characterize the structure and dynamics of the N and U states. This article will not discuss this matter in any detail. The reader is referred to several reviews on the subject (Steiner, 1983; Lakowicz, 1983; Beechem and Brand, 1985; Eftink, 1991). However, I briefly mention that the quantum yield and lifetime of native proteins are not very predictable. Folded proteins can have a quantum yield ranging from 0.03 to 0.4 and nonexponential decays with mean lifetime ranging from 0.5 to 6 ns (Eftink, 1991). Unfolded proteins usually have a quantum yield of about 0.1 and a nonexponential decay with mean lifetime of about 2–3 ns. The fluorescence λ_{max} of a native protein is related to the polarity of the environment of the tryptophan residue and can range from 308–350 nm, with residues in apolar microenvironments having blue emission. Unfolding of a protein almost always leads to a red shift in the emission to a λ_{max} of around 345–355 nm. The anisotropy of a fluorophore depends on the ratio of ϕ_i/τ_i and may either increase or decrease upon unfolding; usually r decreases on unfolding since the rotational correlation time, ϕ_i, is usually smaller for a randomly coiled unfolded protein.

When the change in fluorescence signal between N and U states is not large, tricks that can be played are to add a collisional quencher (such as KI or acrylamide) to the solution, which will usually quench the fluorescence of the unfolded state more than the folded state, or to substitute D_2O as the solvent, which often increases the fluorescence intensity of exposed fluorophores.

Are the N and U states unique?

I also briefly note that fluorescence studies can give some insight about whether the N and U states are single states or a collection of microstates. (Above it was stated that the prompt nature of fluorescence makes it unlikely that there will be any dynamic averaging of a fluorescence signal between two macrostates; this statement may not apply to the dyanamics of the interconversion of microstates.) The basis for the multi-exponential decay of tryptophan residues in peptides and proteins has been discussed by several authors (Alcala et al., 1987*a*, *b*; Vincent et al., 1987). A reasonable model is that the slow interconverion of rotational isomers about the X_1 or X_2 bonds of tryptophan is the molecular basis for the biexponential decay of this simple molecule in solution (with different rotamers having different intramolecular quenching rate constants) (Szabo and Rayner, 1980; Petrich et al., 1983; Chang et al., 1983; Chen et al., 1991). Extending this model to proteins and peptides, a multiexponential decay can be related to the existence of microscopic conformational states (perhaps rotamers of the trp residues), again with different rate constants for the different microstates (Ross et al., 1992; Willis and Szabo, 1992). Alternatively, a nonexponential decay can arise due to dynamic processes that lead to quenching or dipolar relaxation of the excited state. This might involve fluctuations that bring about collisions or approach between amino acid side chains, peptide bonds, solvent molecules, etc. Some intramolecular quenching may involve a distance-dependent electron exchange process, which would produce a nonexponential decay (the latter could cause a nonexponential decay even in the absence of fluctuations and for a single microstate). The interpretations are equivocal in most cases. For an unfolded state, the heterogeneity in the fluorescence decay is usually greater, consistent with the view that the fluorophores in this state experience a variety of microenvironments.

Resonance energy transfer studies have been interpreted to indicate that the DA distance in a native state is not a discrete distance but is a distribution of distances (or a distribution of distances and orientation factors). This supports the notion that a native protein exists as a set of microstates. On

unfolding, the DA distance usually (but not always) shows a broader distribution, as expected for a random coil (Lakowicz et al., 1988; Amir et al., 1992; James et al., 1992).

While the above fluorescence results sense the existence of microscopic states within the N and U macrostates, this does not alter the interpretation of fluorescence signal changes to monitor conformational transitions of proteins. One possible situation where the above microstates might influence the thermodynamic analysis is where there is a progressive shift in the distribution of microstates with addition of denaturant or increase in temperature (Lumry et al., 1966; Shortle and Meeker, 1986). However, it will usually not be possible to distinguish this phenomenon from a baseline trend.

Use of nonlinear least squares and linkages

As mentioned above, we use nonlinear least squares routines to fit thermodynamic models to fluorescence signal changes versus [denaturant] or temperature. We include baseline slopes (linear) for the initial and final states, when it is clear that these baselines do not have a slope of zero.

In many situations, it is useful to analyze several data sets simultaneously in order to test the ability of a thermodynamic model to describe the data. There are a number of examples of data sets that can be linked together for global analysis (Beechem et al., 1992). Some familiar examples include: fluorescence lifetime data obtained at multiple emission wavelength or multiple concentrations of quencher (linkage via Stern-Volmer equation for τ_i), or multiple temperatures (linkage via Arrhenius equation for $1/\tau_i$); fluorescence intensity versus quencher concentration (linkage via Stern-Volmer equation). Below we will present examples of protein unfolding studies in which linkage and global analyses are performed. These linkages are in terms of the van't Hoff plot for temperature dependence studies of protein unfolding, or in terms of Eq. 7 for urea induced unfolding.

The program GLOBALS is useful for many types of global analyses involving time-resolved or frequency-domain fluorescence data (Beechem et al., 1992). For steady-state fluorescence data (or other type of data) we have found the program NONLIN, written by Dr. M. Johnson, to be very useful for global analyses (Johnson and Frasier, 1985; Straume et al., 1992). For routine nonlinear least fitting, we use the commercial programs ENZFITTER (R. J. Leatherbarrow) or SIGMAPLOT 5.0 (Jandel Scientific).

Practical considerations

In this section I mention a number of practical matters related to the use of fluorescence to monitor protein unfolding. It goes without saying that the method used must have a high enough signal/noise ratio to monitor the signal differences between the states. Subtraction of buffer baselines, lamp stability, correction for absorptive screening, correction of spectra for lamp, monochromater, and photomultiplier wavelength-dependent responses, signal averaging and digitizing, minimization of photodegradation, avoidance of Raman and Rayleigh scattering, assurance that the photomuliplier signal is linearly responsive to the concentration of fluorophore, and avoidance of fluorescent contaminant signals are standard procedures and concerns (Parker, 1968; Lakowicz, 1983; Jameson, 1984; Schmid, 1989). Samples should be filtered to minimize light scattering particles and the protein should be shown to be adequately homogeneous to allow meaningful interpretations of results. In the following paragraphs I will discuss practical concerns pertinent to the study of unfolding transitions.

If an unfolding is induced by increasing temperature in a continuous or stepwise manner or by the addition of aliquots of denaturant to a solution, it is important that equilibrium be reached at each new condition before the spectroscopic measurements are made. If equilibrium is not reached, this can result in a distorted transition curve, which will alter the derived thermodynamic parameters (both ΔH°_{un} and T_{un} or $\Delta G^\circ_{o,un}$ and m). Lepock et al. (1992) recently presented a discussion of this problem, with application to scanning calorimetry and I will summarize important points below. The discussion will apply primarily to an experiment in which temperature is increased at a rate of ν (in °C/s), but the concerns also apply to denaturant induced unfolding experiments in which aliquots of denaturant are delivered (for example by a computer controlled syringe pump) in a stepwise manner to a stirred protein solution in a cuvette.

For a reversible two-state $N \rightleftharpoons U$ transition, with forward and reverse rate constants k_1 and k_{-1}, equilibration is achieved if ν is small compared to the relaxation time, $(k_1 + k_{-1})^{-1}$. Using typical values for the thermodynamics and kinetics of protein folding, Lepock et al. simulated data showing a ratio of ν/k_1 less than 10^{-1} to be slow enough to assure equilibration and thus to enable valid recovery of ΔH°_{un} and T_{un}. As an example of when this condition is met, the relaxation time for unfolding of ribonuclease A is about 20 s at its T_{un} of ~50°C at pH 3 (Hagerman and Baldwin, 1976; Mayoraga and Freire, 1987). A thermal scan rate of less than 0.5°C/min would be necessary for equilibrium to be adequately maintained.

If the scan rate is much larger than k_1, then equilibrium is not achieved, and the apparent T_{un} and apparent ΔH° (from van't Hoff analysis) will both be larger than the true values. In fact, analysis of the scan rate dependence and the shape of the transition should enable determination of k_1 and its activation energy (Lepock et al., 1992).

These authors also considered the case in which a reversible unfolding transition is followed by an irreversible denaturation reaction to a state D.

$$N \underset{k_{-1}}{\overset{k_1}{\rightleftharpoons}} U \xrightarrow{k_2} D \tag{22}$$

In general it will be difficult to determine whether such an irreversible denaturation process occurs. Lepock et al. showed that there will still exist a range (that is, a combination of ν, k_1, and k_2) for which a scan rate independence is observed, even with the irreversible step. Only by studying

both the v dependence and shape of the transition can the above two-step mechanism be identified. The effect of the irreversible step will be to cause the apparent T_{un} to be lower, than it would be in the absence of the second step, and to cause the apparent van't Hoff ΔH°_{un} to be larger than its true value. If, however, the denaturation rate constant, k_2, is much lower (i.e., $k_1/k_2 > 10^4$), then the distortion in the thermodynamic parameters will not be significant.

The conclusion is that it is important to use slow scan rates, to test for the scan rate dependence of the apparent T_{un}, and to be cautious about interpreting the shape of thermal transition curves, unless the possibility of an irreversible denaturation has been considered. Since most thermal scanning spectroscopic measurements use water baths and thermojacketed cell holders with a relatively large heat capacity, the scan rates used in such studies is usually not as large as those used in scanning calorimetry. But with thermoelectric cell holders, faster scan rates in spectroscopic studies are now possible and the above concerns should not be ignored. The problem of equilibration in thermal scans will be much greater for a cold unfolding transition of a protein, since the value of k_1 will be much lower than the corresponding k_1 value for a high-temperature transition. Another, related concern with thermal scanning spectroscopic studies is that the temperature be the same at the regions of the cuvette where the light beam is passing and where the thermistor probe is inserted. (It goes without saying that the temperature should always be measured within the cuvette and not in the water bath, since there can be a several degree difference; measurements within the cuvette holder is probably acceptable.) Thermal gradients will be exacerbated by rapid scan rates and may be partially caused by blowing dry gas on one face of a cuvette, but stirring of the sample should minimize such gradients.

The problem of reaching equilibrium in denaturant unfolding experiments must also be considered. One practice used by researchers is to prepare a series of protein solutions having different concentrations of denaturant, let these solutions equilibrate for a period of time (i.e., overnight) and to then read the spectroscopic signal of the series of samples (Pace et al., 1989). Since this serial method is tedious and can introduce pipetting errors, other researchers add aliquots, either by hand or using an automatic syringe pump or peristaltic pump, to a single sample of protein in a cuvette. With the latter method, the experimenter must wait until equilibration is reached, which may be very slow in the transition region. For example, the relaxation time for the urea induced unfolding of ribonuclease T_1 is 6–40 min at 25°C, pH 5 (Thomson et al., 1989); one should wait about 5 times the relaxation time before making a measurement to adequately allow for equilibrium to be reached. Ribonuclease T_1 is an extremely slowly unfolding protein (i.e., the relaxation time for unfolding of Staphylococcal nuclease A is only about 1–2 min at 4.5°C (Sugawara et al., 1991)), but this problem of slow equilibration times for urea and guanidine unfolding limits the advantages of automating these experiments.

One of the main advantages of fluorescence methods is their ability to be used with low concentrations of protein or other fluorophore. In studies where there is a change in the degree of aggregation of the protein upon unfolding (i.e., see below for an example of a dimer to monomer unfolding transition), it is necessary to vary the concentration of protein in order to fully describe the thermodynamics of the process. Even with tryptophan fluorescence, it is possible to approach nanomolar concentrations and still see adequate signal in steady-state fluorescence methods. However, it then becomes important to minimize fluorescence impurities, for example in the buffer components and the urea or guanidine. Pace et al. (1989) has discussed means of purifying these denaturants and the amount of fluorescent impurities that are often found in commercial samples. To measure fluorescence at high concentrations of proteins one must deal with optically thick solutions and problems of aggregation (which may be nonspecific). The use of small-path-length cuvettes or frontal illumination can enable high concentrations to be used.

Heme proteins present special problems and opportunities (Hochstrasser and Negus, 1984; Szabo et al., 1989; Bucci et al., 1988). Since the intrinsic tryptophan fluorescence (of residues near the heme group) is extensively quenched in the native state of heme proteins by energy transfer, the native state of these proteins tend to have a very low fluorescence quantum yield. Consequently, the presence of impurities in the proteins can greatly interfere with the observed fluorescence. Upon unfolding, the fluorescence of heme proteins greatly increases, due to the increase in distance between the tryptophan donors and the heme acceptor; this provides a convenient and large signal change to monitor unfolding.

EXAMPLES

I now present several examples of the use of various fluorescence signals to monitor the thermodynamics and kinetics of proteins. I will discuss a variety of applications and show advantages and disadvantages of the use of different types of signals. Many of the examples will involve Staphylococcal nuclease A and its hybrid mutant, nuclease conA S28G. A comparison of these proteins is useful since they differ greatly in their thermodynamic stability.

Fluorescence intensity versus temperature or denaturant concentration

An example of a thermal unfolding of a protein monitored by steady-sate fluorescence intensity measurement is our study with nuclease A and its mutants (see figure 2 of Eftink et al., 1991a). Upon unfolding the fluorescence quantum yield of nuclease is only about 20% of that of the native form. There is also a red shift upon unfolding. The combination of these effects leads to a very large drop in the fluorescence intensity at 320 nm upon unfolding. Fluorescence intensity (λex = 295 nm; λem = 320 nm) data were collected (via

digital acquistion every minute) as a function of temperature with a scan rate of about 0.5°C/min (reading a thermistor inserted in the cuvette). We have used nonlinear least squares to fit the F versus T curves to the following equation, which is a combination of Eqs. 4, 5, and 14b.

$$F = \frac{F_{oN} + s_N T + [F_{oU} + s_U T] \cdot e^{(-\Delta H^\circ_{un} + T\Delta S^\circ_{un})/RT}}{1 + e^{(-\Delta H^\circ_{un} + T\Delta S^\circ_{un})/RT}} \quad (23)$$

Fitting this equation (using ENZFITTER or NONLIN) to data involves six fitting parameters, the fluorescence intensities of the native state, F_{oN}, and the unfolded state, F_{oU}, at some reference temperature (0°C), the temperature dependence (i.e., baseline slope, assumed to be linear) of the fluorescence of the native state, s_N, and unfolded state, s_U, the enthalpy change, ΔH°_{un}, and the entropy change, ΔS°_{un}, for the two-state unfolding reaction. The fits to the two-state model are very good and the fitting parameters were found to have small confidence intervals.

A couple of the mutants that were studied have very low thermodynamic stability and show a tendency expected for cold unfolding. Fig. 2 of Eftink et al. (1991a) shows the fluorescence to increase slightly with increasing temperature in the range of 2–15°C. Care was taken to scan the temperature more slowly in this low temperature range. The data for these mutants were analyzed to obtain an additional thermodynamic parameter, the heat capacity change, $\Delta C_{p,\,un}$, for unfolding. That is, Eq. 21 was expanded to

$$F = \frac{\begin{aligned} &F_{oN} + s_N T + [F_{oU} + s_U T] \\ &\quad \cdot \exp[(-\Delta H^\circ_{oun} - \Delta C_{pun}(T - T_{un}) \\ &\qquad + T\Delta S^\circ_{oun} + T\Delta C_{pun}\ln(T/T_{un}))/RT] \end{aligned}}{\begin{aligned} &1 + \exp[(-\Delta H^\circ_{oun} - \Delta C_{pun}(T - T_{un}) \\ &\qquad + T\Delta S^\circ_{oun} + T\Delta C_{pun}\ln(T/T_{un}))/RT] \end{aligned}} \quad (24)$$

We performed a nonlinear least-squares fit to obtain $\Delta C_{p,\,un}$ values of 2680 cal/mol·deg, a value that is similar to that obtained for the wild-type protein by calorimetric studies (Griko et al., 1988). This analysis of F versus T to obtain a $\Delta C_{p,\,un}$ value requires the assumption that the fluorescence intensity (at the reference temperature) of the cold-unfolded state is that for the high temperature unfolded state (i.e., that there is a linearly sloping baseline that connects both unfolded states). Without this assumption, it will be nearly impossible to obtain fits for both $\Delta C_{p,\,un}$ and for a fluorescence for the cold unfolded state (that is different from that for the high temperature unfolded state).

Measurement of F versus [urea] or [guanidine] has become a standard method for studying the stability of proteins. The following equation (a combination of Eqs. 4, 7, and 14b, with inclusion of baseline slopes) describes such data:

$$F = \frac{F_{oN} + s_N[D] + (F_{oU} + s_U[D]) \cdot e^{(-\Delta G^\circ_{o,un} + m[D])/RT}}{1 + e^{(-\Delta G^\circ_{o,un} + m[D])/RT}} \quad (25)$$

In this equation, F_{oN} and F_{oU} are the intensities of the native and unfolded states in the absence of denaturant, s_N and s_U are the baseline slopes for the native and unfolded regions, and $\Delta G^\circ_{o,\,un}$ and m are defined in Eq. 7. Pace et al. (1989) have described technical aspects of such measurements. In our lab we use manual methods for adding denaturant, due to the concern about reaching equilibrium. Either we add aliquots from a concentrated stock solution of denaturant to a cuvette containing protein, or we use a Job method by preparing and then mixing two solutions, one which contains protein but no denaturant and the other which contains the same concentration of protein and a high concentration of denaturant. By doing Job titrations upwards and downwards we can test for reversibility of the unfolding transition. Usually the baseline slope for the native state is small when urea is the denaturant, whereas the slopes for the unfolded state is usually a larger, positive value (as expected from the model study in Fig. 7) for both urea and guanidine-HCl. The baseline slope for the native state with guanidine as denaturant has been found to be both near zero in some cases and to be a large positive value in other cases. The latter instances, which include ribonuclease T_1 and barnase, have been interpreted in terms of the specific binding of guanidine to the protein, with the induction of a slight change in fluorescence (Pace et al., 1990).

Some researchers use automatic titrators to add denaturant, which enables a high density of data to be collected (Saito and Wada, 1983), but this may lead to problems of equilibration mentioned above.

Intensity decays versus temperature or denaturant concentration

If the intrinsic decay times of the native and unfolded states are significantly different, then the pre-exponentials associated with these τ_i values can be related to the fraction of molecules in the native and unfolded states. While in principle this is so, in practice the decay of a pure states can be a multiexponential and the assignment of τ_i components to species can be difficult. In our study of the thermal unfolding of nuclease A and its mutants (Eftink et al., 1991b), we found the intensity decays to be a bi- or triexponential and that the long decay time tracked the population of native states and that the shortest decay time tracked the population of unfolded states. An intermediate decay time seemed to have some weight in each species. We performed a global analysis (using GLOBALS) of several intensity decay data sets (at temperatures from 10–60°C) in terms of a triexponential decay law, with the τ_i at various temperatures being linking by an Arrhenius relationship, $1/\tau_i = A_i \exp(-E_{a,\,i}/RT)$. The recovered α_i values for the three τ_i were then analyzed according to a two-state unfolding model via Eq. 5. Analysis of the α_i for the longest and shortest τ_i gave values of ΔH°_{un} and ΔS°_{un} that are in agreement with thermodynamic values determined by separate scanning calorimetric studies or from measurement of the fluorescence intensity versus T.

We have also measured the fluorescence decay of nuclease A and its thermodynamically unstable mutant, nuclease conA S28G, as a function of the concentration of guanidine-HCl (Eftink and Wasylewski, 1992). The τ_i and α_i from fits of a biexponential decay law to each data set are plotted in

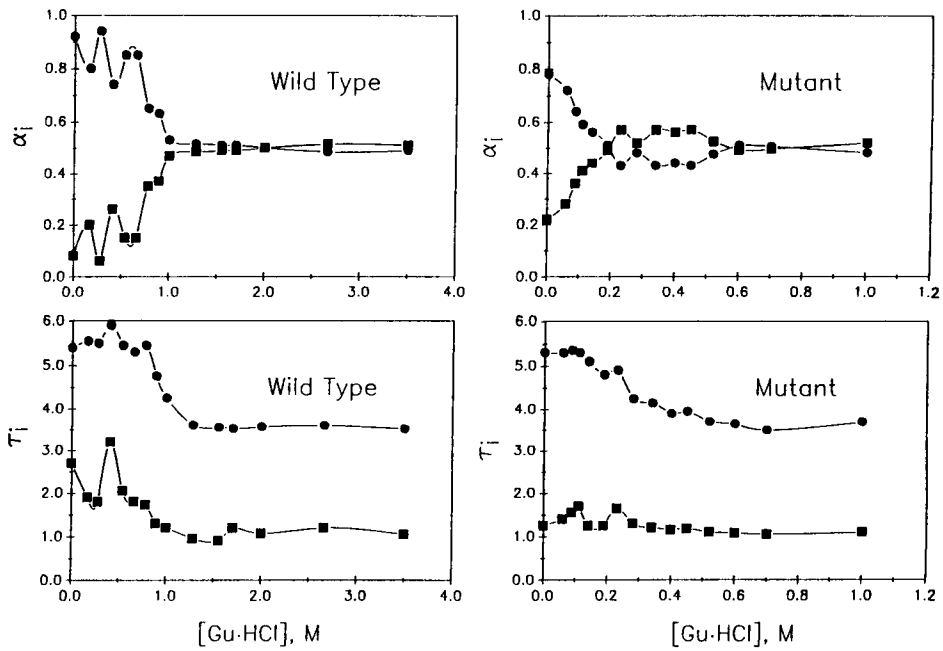

FIGURE 9 The dependence of the pre-exponentials, α_i, and lifetimes, τ_i (for a bi-exponential decay law), of Staphylococcal nuclease A and mutant NCA S28G on the concentration of guanidine-HCl. Measurements made at 20°C and pH 7, 0.01 M Tris-HCl, 0.1 M NaCl buffer using a phase modulation fluorometer. Excitation at 300 nm, emission collected through a WG320 filter. Data taken from Eftink and Wasylewski, 1992.

Fig. 9 as a function of [guanidine]. As with our temperature studies, the longest τ_i seems to be characteristic of the native state and the shortest τ_i seems to be characteristic of the unfolded state, with the respective α_i tracking the population of states. We performed a global analysis of intensity decay data sets at 15 concentrations of guanidine-HCl, by linking the τ_i to a triexponential decay law. Fig. 10 shows the resulting α_i for the global fit. These α_i were then fitted via equation 7 to obtain the free energy of unfolding of the protein in the absence of denaturant, $\Delta G^\circ_{o,un}$, and the denaturant index, m. Values of the latter parameters were found to be in agreement with values determined from measurements of steady-state fluorescence versus [guanidine]. Thus, in favorable cases such as nuclease A and its mutants, where there is a significant difference in the dominant τ_i for the native and unfolded states, time-resolved intensity decay data can be used to determine thermodynamic parameters for a temperature or denaturant induced unfolding of a protein. Admittedly, time-resolved fluorescence is an instrument intensive way to obtain such information.

The above analyses were based on the use of discrete exponential to describe the intensity decays. Another way to analyze fluorescence decay data is in terms of a distribution of decay times (Alcala et al., 1987*a*, *b*). A unimodal distribution is often sufficient to fit a moderately nonexponential decay. When the decay is very nonexponential, a bimodal distribution of decay times may be needed. As a protein is unfolded by temperature or denaturant, it is likely that the intensity decay will become more nonexponential, due to the presence of different states with different mean τ. If one still analyzes such data in terms of a unimodal distribution, the width of this distribution will increase in the transition range (see Fig. 11 *A* and figure 2 of Eftink et al., 1989). A quantitative analysis, in terms of a distribution model, to obtain thermodynamic data can be performed. For example, we performed a global analysis of the decay data sets obtained for nuclease A and its mutant at various [guanidine], with the decays of the pure states being described by a unimodal distribution (so there would be a bimodal distribution in the transition range). The mean τ for the native state was long (4.99 ns), and the mean τ for the unfolded state was short (1.85 ns). In the linked analysis, we assumed the distribution width, Δ_i, to be constant at all [guanidine] for the two states. The analysis was done using GLOBALS; the α_i for the two states versus [guanidine] are shown in Fig. 11 for nuclease A and the mutant NCA S28G. Analysis of the α_i versus [guanidine] parameters via Eq. 7 provides ΔG°_{un} and m values that are very similar to values obtained via steady-state fluorescence versus [guanidine]. I raise a point about the GLOBALS program and the way it fits a distribution model. The amplitude factors can be toggled between being pre-exponential α_i values and fractional fluorescence intensity values. It is the former that track the population of species.

We have also attempted a distribution analysis of our intensity decay versus T data sets. Here, however, the analysis is more difficult that expected. If linkage of the temperature data sets is in terms of an Arrhenius equation, then the shape of a distribution pattern will actually change as temperature is changed. (This is because long τ components within the distribution are quenched more than are shorter τ components with an increase in temperature.) We have not been satisfied with our attempts to fit such intensity decay versus T data in terms of a bimodal distribution model.

Fluorescence anisotropy versus temperature or denaturant concentration

Since the steady-state emission anisotropy, r, is likely to change upon unfolding of a protein, due to changes in either/both the fluorescence decay time or rotational correlation

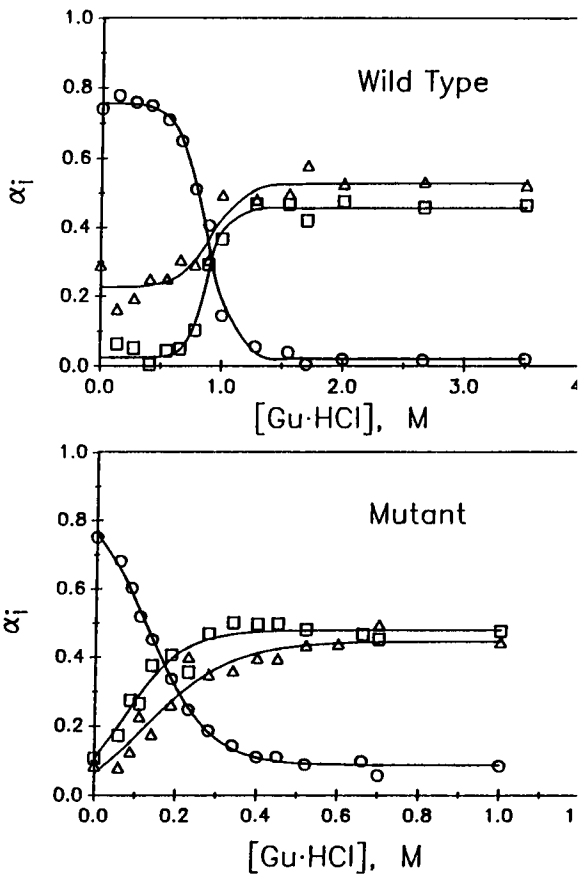

FIGURE 10 Pre-exponentials for the long (○, 5.6 ns), medium (△, 3, 3 ns), and short (□, 1.0 ns) lifetimes for a tri-exponential decay fit of the data in Fig. 9 (listed τ_i values are for the wild type; similar values are found for the mutant NCA S28G). The α_i values are obtained from a global analysis of the data sets. The solid lines are a subsequent analysis of the α_i values in terms of Eq. 5. For the longest τ, we obtain $\Delta G^\circ_{o,un}$ = 4.6 ± 0.5 kcal/mol and m = 5.27 ± 0.56 kcal·liter/mol² for the wild type and $\Delta G^\circ_{o,un}$ = 0.98 ± 0.15 kcal/mol and m = 7.6 ± 0.6 kcal·liter/mol² for the mutant.

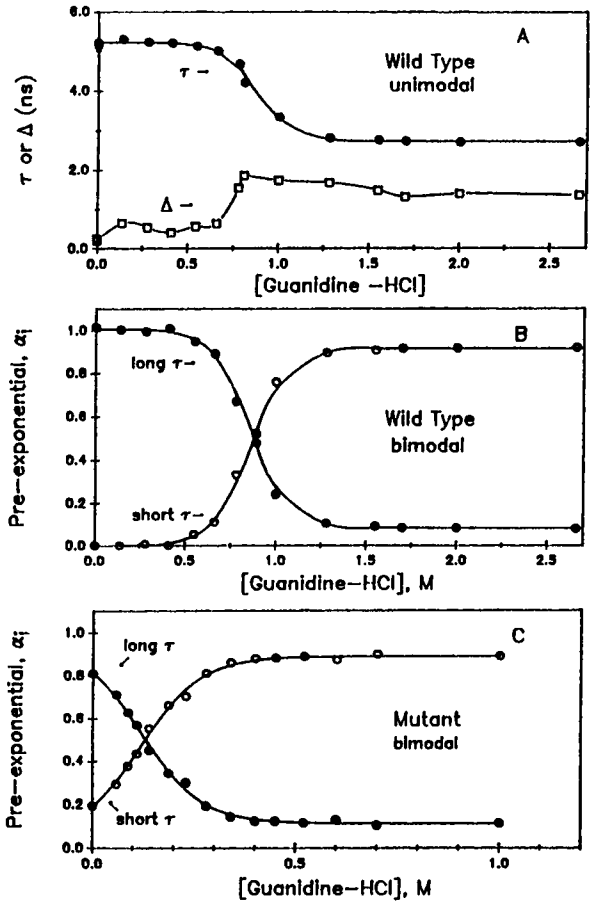

FIGURE 11 (*A*) Plot of the mean lifetime (●) and width (□) for a unimodal Lorentzian distribution analysis of the fluorescence decay of wild-type nuclease A as a function of the concentration of guanidine-HCl. The solid line through the mean lifetime data is a fit to Eq. 25 with $\Delta G^\circ_{o,un}$ = 4.99 ± 0.06 kcal/mol and m = 5.69 ± 0.05 kcal·liter/mol². The lines through the widths have no theoretical significance. (*B*) Plot of the amplitude for the long (τ_1 = 4.99 ns, Δ_1 = 1.0 ns) and short (τ_2 = 1.85 ns, Δ_2 = 1.16 ns) lifetimes for a bimodal Lorentzian distribution analysis of the fluorescence decay of wild-type nuclease as a function of the concentration of guanidine-HCl. The solid lines are a fit with $\Delta G^\circ_{o,un}$ = 4.60 ± 0.04 kcal/mol and m = 5.40 ± 0.04 kcal·liter/mol². (*C*) Plot of the amplitude for the long (τ_1 = 5.03 ns, Δ_1 = 1.0 ns) and short (τ_2 = 1.74 ns, Δ_2 = 1.14 ns) lifetimes for a bimodal Lorentzian distribution analysis of the fluorescence decay of nuclease conA S28G mutant as a function of the concentration of guanidine-HCl. The solid lines are a fit with $\Delta G^\circ_{o,un}$ = 0.94 ± 0.02 kcal/mol and m = 7.89 ± 0.06 kcal·liter/mol².

time, measurement of r versus T or [denaturant] will usually monitor the unfolding transition. However, as discussed above, the r values do not directly track the fraction of molecules in the native and unfolded states, but are weighted by the relative fluorescence intensity of the two states. The baseline regions for the pure states will usually have smaller slopes, as compared to fluorescence intensity measurements, since r is determined by the ratio of τ_i/ϕ_i, and the τ_i and ϕ_i in this ratio should have roughly the same temperature dependence. Other drawbacks of r measurements are that the signals will be noisier than simple intensity measurements, due to the reduction in transmitted light by the polarizers, and that there is a need to rotate, either manually or automatically, the polarizers. The latter makes such measurements a little more cumbersome to perform. (Alternately, a researcher can use a "T" format with two emission channel, one for parallel and the other for perpendicular emission.)

Shown in Fig. 12 is a measurement of r versus [guanidine-HCl] for the unfolding of nuclease A_1. There is an adequate difference between the r values for the native and unfolded states and the baseline regions have essentially a linear slope. We performed a nonlinear least-squares analysis of these data using a combination of Eqs. 4, 7, and 16b. The resulting $\Delta G^\circ_{o,un}$ value from analysis of the r data is slightly larger than the value obtained from analysis of fluorescence intensity data, as expected from the discussions relating to the simulations under Thermodynamic Models for the Unfolding of a Protein, above.

Anisotropy decay versus temperature or [Denaturant]

The anisotropy decay of an unfolded protein will usually be more rapid than that of a native protein, due to the flexibility

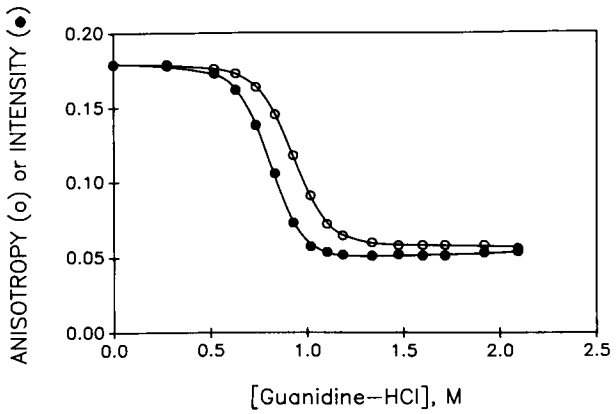

FIGURE 12 Steady-state fluorescence intensity (●) and anisotropy (○) measurements for Staphylococcal nuclease A as a function of the concentration of guanidine-HCl at 20°C, pH 7, 0.01 M Tris-HCl, 0.1 M NaCl. Excitation at 300 nm, emission through a bandpass filter centered at 350 nm. The solid line through the intensity data is a fit of Eq. 25 with $\Delta G^{\circ}_{o,un}$ = 5.67 ± 0.02 kcal/mol and m = 6.92 ± 0.03 kcal·liter/mol^2. The solid line through the anisotropy data is for $\Delta G^{\circ}_{o,un}$ = 5.98 ± 0.02 kcal/mol and m = 6.40 ± 0.02 kcal·liter/mol^2.

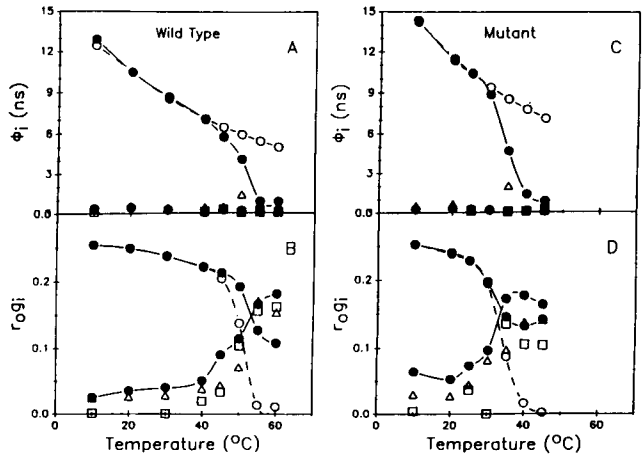

FIGURE 13 (*A*) Plot of ϕ_i versus T for wild-type nuclease A (data from figure 6 of Eftink et al., 1991b). Closed symbols, unconstrained, nonassociated biexponential anisotropy decay law. Open symbols, triexponential anisotropy decay law, with ϕ_1 constrained to have an Arrhenius dependence on temperature and with ϕ_1 "associated" with the two longer τ_i values for the fluorescence decay of the protein (see Eftink et al., 1991b), with ϕ_3 "associated" with the two shortest τ_i and with ϕ_2 "associate" with all τ_i components. (*B*) Plot of $r_o g_i$ versus T for wild-type nuclease A. Symbols are indicated above. (*C*) Plot of ϕ_i versus T for nuclease conA S28G mutant (data from figure 7 of Eftink et al., 1991b). Closed symbols are for an unconstrained, nonassociated biexponential anisotropy decay law. Open symbols are for a constrained, "associated" triexponential decay law, as indicated above. (*D*) Plot of $r_o g_i$ versus T for mutant. Symbols as indicated above. The constrained ϕ_1 were forced to be described by an Arrhenius equation, $\phi_1^{-1} = A \cdot \exp(-E_a/RT)$. Values of E_a = 3.52 kcal/mol and $A = 3.71 \times 10^9$ were determined from the 10–40°C data for wild-type nuclease A.

of the indole side chain in a random coil. When there is a mixture of folded and unfolded states, the anisotropy decay function is complicated (see Eq. 19), and analysis is made more difficult by the fact that the anisotropy decay law for each state may be a nonexponential and the ϕ_i values should be "associated" with certain τ_i values.

To illustrate such data and the problems of analysis, consider the anisotropy decays for nuclease A, and one of its mutants, as a function of temperature, as shown in figures 6 and 7 of Eftink et al. (1991b). If such data are fitted to a biexponential anisotropy decay law (see Tables V and VI of above reference), the fits are adequate and the resulting ϕ_i and $r_o g_i$ versus temperature are shown in Fig. 13. The values of $r_o g_1$ and $r_o g_2$ decrease and increase, respectively, with increasing temperature for both wild type and mutant proteins, suggesting that these parameters are tracking the unfolding transitions. However, the value of $r_o g_1$ does not drop to zero as the transition is completed for either protein. The value of ϕ_1 also decreases with temperature, as shown in Fig. 13, *A* and *C*. This latter pattern is not what is expected for a two-state transition, however. For a two-state transition, the ϕ_i values should be characteristic of the N and U states, and the amplitude ($r_o g_i$) associated with these ϕ_i should track the population of the N and U states. The ϕ_i should not go through a transition, as appears to be the case in Fig. 13, *A* and *C*. The problem is that the data were fitted to a biexponential decay law, which apparently is not adequate to properly describe the data (i.e., both the N and U states may have nonexponential anisotropy decays) and the analysis included no "association" between the ϕ_i and τ_i components.

The anisotropy decay data for wild-type and mutant nuclease have also been analyzed by fixing the longest rotational correlation time, ϕ_1, to have an Arrhenius temperature dependence (with activation energy and Arrhenius factor for ϕ_1^{-1} being that for the 10–40°C data for the wild-type nuclease A), by using a triexponential anisotropy decay law, and by associating the ϕ_1 value with the longest fluorescence lifetime component (since the long lived component seems to also track the population of the N state). This second analysis is shown as the open symbols in Fig. 13. Constraining ϕ_1 to have an Arrhenius behavior makes the ϕ_i values more realistic, and the resulting $r_o g_1$ values drop to zero as the unfolding transition is completed (as is expected if ϕ_1 tracks the N state). Likewise, the $r_o g_2$ and $r_o g_3$ values increase as the unfolding transition occurs. While this analysis is very complicated and requires many assumptions, the point is that the anisotropy decay data are consistent with a two-state unfolding transition.

Fluorescence resonance energy transfer studies

This method, together with an analysis in terms of a distribution of distances, has been used by several researchers to characterize the donor-to-acceptor distance in native and unfolded forms of proteins (Lakowicz et al., 1988; James et al., 1992). Amir et al. (1992) has shown that, with an equilibrium mixture of unfolded and native-like states, a bimodal distance distribution can be determined for segments of pancreatic trypsin inhibitor. This analysis is a state-of-the-art study and it is probably not realistic to use this type of measurement to obtain thermodynamic information for protein unfolding.

Linked equilibria: protein or ligand concentration dependence in unfolding transitions

For the unfolding of oligomeric proteins, the apparent thermodynamic parameters for thermal or denaturant induced unfolding will depend on the total concentration of protein subunits, $[M]_o$. For example, for the denaturant induced unfolding of a dimeric protein (the simplest case), the free energy change for unfolding and the fraction of unfolded molecules are given by Eqs. 27 and 28

$$D \rightleftharpoons 2U; \qquad K_{un} = [U]^2/[D] \tag{26}$$

$$\Delta G^\circ_{un} = -RT \ln K_{un} \tag{27}$$

$$X_{un} = [(K^2_{un} + 8K_{un}[M]_o)^{1/2} - K_{un}]/(4[M]_o) \tag{28}$$

where K_{un} is the equilibrium constant for the unfolding of the native dimer to two unfolded monomers, ΔG°_{un} is the intrinsic unfolding free energy change, $[M]_o$ is the total concentration of protein expressed as monomers. If the unfolding of such a dimeric protein were incorrectly analyzed (using Eqs. 23 or 25 for thermal and denaturant induced unfolding), the apparent ΔG°_{un}(app) would depend on subunit concentration. There are a number of examples of the application of Eq. 28 to characterize the unfolding of an oligomeric protein (Grant et al., 1992; Timm and Neet, 1992). For example, Gittelman and Matthews (1990) have shown the urea induced unfolding of dimeric trp aporepressor to be described by the above equations over a $[M]_o$ range of 5 to 60 micromolar subunits at neutral pH. A global analysis of unfolding data at multiple $[M]_o$ can be performed.

A second type of linked equilibrium is the binding of a specific ligand. It is usually the case that a ligand will bind to the native state and not to the unfolded state of a protein. For the following equilibrium, the apparent free energy change for denaturant unfolding is

$$\begin{array}{ccc} & N \rightleftharpoons U & \\ L & \updownarrow & \\ & N \cdot L & \end{array} \tag{29}$$

$$\Delta G^\circ_{un}(app) = -RT \ln K_{un} + RT \cdot \ln(1 + K_L[L]) \tag{30}$$

$$X_U = K_{un}/(1 + K_{un} + K_L[L]) \tag{31}$$

where K_L is the association constant of ligand and [L] is the free ligand concentration. (If the ligand can also bind to the U state with association constant K'_L, the last term in Eq. 30 becomes $RT \cdot \ln((1 + K_L[L])/(1 + K'_L[L]))$.) From measurements of a fluorescence signal change as a function of temperature or denaturant concentration, data can be analyzed to obtain both ΔG°_{un} (and ΔH°_{un} or m, depending on the type perturbation used to unfold the protein) and the free energy change for ligand binding, $\Delta G^\circ_L = -RT \cdot \ln K_L$. Again, global analysis of multiple data sets in terms of Eq. 31 is possible. In principle, one should be able to use Eq. 31 to determine extremely large values of K_L, just as differential scanning calorimetry studies as a function of [L] have been able to yield K_L values as large as 10^{20} M^{-1} (Sturtevant, 1987; Brandts and Lin, 1990). (Note that with such large K_L values, the time needed to reach equilibrium may be very long, which may distort the unfolding profiles.) An example of a study of the denaturant induced unfolding of a protein in the presence and absence of a specific ligand is the work by Hynes et al. (1989) and Sugawara et al. (1991) with nuclease and the ligand deoxythymidine-3′,5′-diphosphate. Also, Pace and Grimsley (1988) used the above model to determine the weak binding constants for the interaction of cations and anions with ribonuclease T_1.

Deviations from two-state unfolding transitions

The above discussions have assumed the unfolding transitions to be two-state. In fact, one of the goals of studies of protein unfolding is to determine the energetics and mechanism of folding steps and to discern if there are intermediates in the process. Kinetic studies have a greater chance of identifying intermediates. Thermodynamic studies can determine the stability of any intermediates and can potentially describe the energetics of the interaction between and unfolding of domain regions.

The question is whether the unfolding is two-state or whether it must be described by a three- (or multi-) state mechanism, such as that below.

$$N \rightleftharpoons I \rightleftharpoons U \tag{32}$$

Examples of studies that have revealed such a mechanism are the work of Saito et al. (1983) and Palleros et al. (1993). Although using another spectroscopic technique, Barrick and Baldwin (1993) have presented models for the analysis of a three-state unfolding of apomyoglobin.

Characterization of the thermodynamics of a two step process can be difficult, particulary if the population of the intermediate is very low and if the signal of the intermedieate is similar to that of either the N or U states. The population of I and its signal can be inversely and highly correlated. Another consideration is that, if only a single fluorescent center is used to monitor the unfolding transition and if the protein has multiple folding domains, this probe may only be sensitive to transitions in its own domain.

Combination of fluorescence methods with other methods

A strategy used in our laboratory and others is to combine different types of data to monitor the same structural transition. For example, we have developed a multidimensional spectrophotometer, which will simultaneously monitor the circular dichroism, absorbance, and steady-state fluorescence of a sample. Using a computer-controlled thermoelectric sample holder, we can perform thermal scans and collect multiple types of data to monitor the unfolding of a protein. By also measuring the standard deviation of each type of data, we perform properly weighted nonlinear least-squares

fitting of unfolding models to the multiple data sets (Ramsay and Eftink, 1994).

The use of multiple monitoring methods is, of course, a strategy in trying to determine whether a transition is two-state or multistate (Lumry et al., 1966). In doing so it is essential that each monitoring method track the population of states in a linear manner. For example, if circular dichroism is combined with a fluorescence method, the latter should be a parameter that is related to X_U by Eq. 12 (i.e., the parameter should not be changes in fluorescence λ_{max}, anisotropy, or average τ).

Pressure-induced transitions

We have focused on thermal and denaturant induced unfolding transitions, since these are the most commonly performed. Another intensive variable that can induce protein unfolding is hydrostatic pressure. The free energy change for protein unfolding at 1 atm, $\Delta G^\circ_{o,un}$ (1 atm), and the volume change, ΔV_{un}, for the pressure-induced unfolding of a monomeric protein are given by the following:

$$\Delta G^\circ_{un}(P) = \Delta G^\circ_{o,un}(1 \text{ atm}) + P\Delta V_{un} \quad (33)$$

Classical studies of pressure unfolding of proteins were performed in the late 1960s and early 1970s (Gill and Glogovsky, 1965; Brandts, et al., 1970; Zipp and Kauzmann, 1973) and Weber's group has studied the use of pressure to induce the dissociation of oligomeric proteins (Paladini and Weber, 1981; Weber and Drickamer, 1983; Royer et al., 1986). Recent studies of pressure induced unfolding of proteins have characterized the $\Delta G^\circ_{o,un}$ and ΔV_{un} for the pressure induced unfolding of nuclease A and some of its mutants (Eftink et al., 1991a; Royer et al., 1993). Although the kinetics of pressure induced unfolding and the pressure dependence of baseline signals for the pure states have not been thoroughly investigated, the studies to date do not suggest these to be significant problems.

An example of data for the fluorescence of the NCA S28G mutant of nuclease A as a function hydrostatic pressure is shown in figure 4 of Eftink et al. (1991a). The sample was thermostated at 20°C within a high-pressure cell. The data show that the raw fluorescence phase angle (for frequency domain measurements, with modulation frequency ω, of 50 MHz) of the protein decreases as pressure is increased in a way that appears to track the conformational transition. Phase angles were measured for practical reasons. The pressure experiments span several hours and in some cases can involve the repositioning of the pressure cell; this makes relative intensity studies difficult. The phase angle is related to the apparent fluorescence lifetime and we find phase angle data to be very stable and reproducible. In our earlier analysis of these data (Eftink et al., 1991a), we assumed (incorrectly—see below) that the changes in the phase angle linearly track the unfolding transition. We analyzed the data (using Eqs. 4, 14b, and 33) to obtain values of $\Delta G^\circ_{o,un} = 1.25$ kcal/mol and a value of $\Delta V_{un} = -124$ ml/mol. Similar thermodynamic results (using fluorescence intensities) have recently been reported by Royer et al. (1993) for the pressure-induced unfolding of other mutants of nuclease.

Actually, the apparent phase angle, Θ_ω, for a mixture of species is weighted toward the species having the longer fluorescence lifetime by the following series of equations (Lakowicz, 1983) (where it is assumed that the entire emission envelope is observed).

$$\Theta_\omega = \tan^{-1}(N_\omega/D_\omega) \quad (34)$$

where

$$N_\omega = \frac{\sum X_i\omega\tau_i^2/(1 + \omega^2\tau_i^2)}{\sum X_i\tau_i} \quad (35)$$

and

$$D_\omega = \frac{\sum X_i\tau_i/(1 + \omega^2\tau_i^2)}{\sum X_i\tau_i} \quad (36)$$

Combining Eqs. 4 and 33–36, a more rigorous description of apparent Θ_ω versus P data can be obtained with the fitting parameters $\Delta G^\circ_{o,un}$, ΔV_{un}, τ_N, and τ_U. On doing this with the data in figure 4 of Eftink et al. (1991a), we obtain a fit that is as good as that shown in the original figure; the new set of fitting parameters are $\Delta G^\circ_{o,un} = 1.04 \pm 0.21$ kcal/mol and $\Delta V_{un} = -124 \pm 17$ ml/mol (and with the N and U states having mono-exponential decays of $\tau_N = 4.96$ ns and $\tau_U = 2.25$ ns). This $\Delta G^\circ_{o,un}$ value is 20% smaller than the value reported in the previous paragraph (obtained with the false assumption that Θ_ω linearly tracks the transition). This demonstrates that, to obtain valid thermodynamic data from fluorescence data, either the fluorescence signal must obey Eq. 12 or a more complicated analysis procedure must be used to relate the signals to values of X_i though the transition.

SUMMARY

The simulations and discussions in this article raise the following points about the use of fluorescence methods to monitor conformational transitions:

a. Fluorescence lends itself to such studies because it is a multidimensional method, and it is likely that some fluorescence signals will be different upon a conformational change, due to the sensitivity of the fluorescence of a chromophore to its microenvironment.

b. Among the various fluorescence signals that can be measured, it is important to use those that are directly related to the mole fraction of states of the protein (i.e., $\mathbf{S} = \sum X_i\mathbf{S}_i$). These signals are the steady-state fluorescence intensity, apparent quantum yield, pre-exponential factors for intensity decay, and mean fluorescence lifetime. Other signals, including the emission λ_{max}, anisotropy, and average fluorescence lifetime are weighted toward the more intensely emitting species and do not directly track the mole fraction of states.

c. In using any of the fluorescence signals to monitor a conformational transition, it is important to realize that there

may be changes in the absorption spectra as well, and, unless an isosbestic wavelength is used, the difference in absorption probability will be factored into the fluorescence changes and will give rise to small errors in derived thermodynamic parameters.

d. Whether using chemical denaturants or temperature as perturbant, baseline slopes must be included in the analysis. Even for temperature studies, it will almost always suffice to assume linear baselines for the pure states. If a baseline region is not well defined, a slope from a study with a model system can be used. In cases where the protein is marginally stable and does not exist as ~100% folded under any condition, the signal for the completely folded state should not be simply taken as the value at minimum perturbation. Nonlinear least-squares procedures should be used and the signal for the folded state should be considered an unknown fitting parameter.

e. The existence of a cold unfolding transition must be considered in cases where studies are made at low temperatures or for marginally stable proteins.

f. When using automated data acquisition procedures, it is important to assure that the unfolding transition reaches equilibrium before measurements are acquired.

This research was supported by NSF grant DMB 91-06377.

REFERENCES

Alcala, J. R., E. Gratton, and F. G. Prendergast. 1987a. Fluorescence lifetime distributions in proteins. *Biophys. J.* 51:597–604.

Alcala, J. R., E. Gratton, and F. G. Prendergast. 1987b. Interpretation of fluorescence decays in proteins using continuous lifetime distributions. *Biophys. J.* 51:925:936.

Amir, D., S. Krausz, and E. Haas. 1992. Detection of local structures in reduced unfolded bovine pancreatic trypsin inhibitor. *Proteins Struct. Funct. Genet.* 13:162–173.

Barrick, D., and R. L. Baldwin. 1993. Three-state analysis of sperm whale apomyoglobin folding. *Biochemistry* 32:3790–3796.

Becktel, W. J., and J. A. Schellman. 1987. Protein stability curves. *Biopolymers* 26:1859–1877.

Beechem, J. M., and L. Brand. 1985. Time resolved fluorescence decays in protiens. *Annu. Rev. Biochem.* 54:43–71.

Beechem, J. M., E. Gratton, M. Ameloot, J. R. Knutson, and L. Brand. 1991. The global analysis of fluorescence intensity and anisotropy decay data: second-generation theory and programs. *In* Fluorescence Spectroscopy: Principles. Vol. II. J. R. Lakowicz, editor. Plenum Press, New York. 241–305.

Biltonen, R. L., and E. Freire. 1978. Thermodynamic characaterization of conformational states of biological macromolecules using differential scanning calorimetry. *CRC Crit. Rev. Biochem.* 5:85–124.

Brandts, J. F., C. Q. Hu, L-N. Lin, and M. T. Mas. 1989. A simple model for proteins with interacting domains. Applications to scanning calorimetry data. *Biochemistry.* 28:8588–8596.

Brandts, J. F., and L-N. Lin. 1990. Study of strong to ultrastrong protein interactions using differential scanning calorimetry. *Biochemistry.* 29: 6927–6940.

Brandts, J. F., R. J. Oliveria, and C. Westwort. 1970. Thermodynamics of protein denaturation. Effect of pressure on the denaturation of ribonuclease A. *Biochemistry.* 9:1038–1047.

Bucci, E., H. Malak, C. Fronticelli, I. Gryczynski, and J. R. Lakowicz. 1988. Resolution of the lifetime and correlation times of the intrinsic tryptophan fluorescence of human hemoglobin solutions using 2 GHz frequency-domain fluorometry. *J. Biol. Chem.* 263:6972–6977.

Chang, M. C., J. E. Petrich, D. B. McDonald, and G. R. Fleming. 1983. Nonexponential fluorescence decay of tryptophan, tryptophylglycine, and glycyltryptophan. *J. Am. Chem. Soc.* 105:3819–3824.

Chauvin, F., D. Toptygin, S. Roseman, and L. Brand. 1992. Time-resolved intrinsic fluorescence of enzyme I. The monomer/dimer transition. *Biophys. Chem.* 44:163–173.

Chen, R. F., J. R. Knutson, H. Ziffer, and D. Porter. 1991. Fluorescence of tryptophan dipeptides: correlations with the rotamer model. *Biochemistry.* 30:5184–5195.

Eftink, M. R. 1991. Fluorescence techniques for studying protein structure. *Methods Biochem. Anal.* 35:127–205.

Eftink, M. R., C. A. Ghiron, R. A. Kautz, and R. O. Fox. 1991a. Fluorescence and conformational stability studies of Staphylococcus nuclease and its mutants, including the less stable nuclease-concanavalin A hybrids. *Biochemistry.* 30:1193–1199.

Eftink, M. R., I. Gryczynski, W. Wiczk, G. Laczko, and J. R. Lakowicz. 1991b. Effects of temperature on the fluorescence intensity and anisotropy decays of Staphylococcal nuclease and the less stable nuclease-conA-SG28 mutant. *Biochemistry.* 30:8945–8953.

Eftink, M. R., and Z. Wasylewski 1992. Time-resolved flurescence studies of the thermal and guanidine induced unfolding of nuclease A and its unstable mutants. *SPIE Proc.* 1640:579–584.

Egan, D. A., T. M. Logan, H. Liang, E. Matayoshi, S. W. Fesik, and T. F. Holzman. 1993. Equilibrium denaturation of recombinant human FK binding protein in urea. *Biochemistry.* 32:1920–1927.

Fernando, T., and C. A. Royer. 1992. Unfolding of *trp* repressor studied using fluorescnece spectroscopic techniques. *Biochemistry.* 31: 6683–6691.

Gill, S. J., and R. L. Glogovsky. 1965. Influence of pressure on the reversible unfolding of ribonuclease and polybenzyl-L-glutamate. *J. Phys. Chem.* 69:1515–1519.

Gittelman, M. S., and C. R. Matthews. 1990. Folding and stability of *trp* aporepressor from *Escherichia coli. Biochemistry.* 29:7011–7020.

Grant, S. K., I. C. Deckman, J. S. Culp, M. D. Minnich, I. S. Brooks, P. Hensley, C. Debrouck, and T. D. Meek. 1992. Use of protein unfolding studies to determine the conformational and dimeric stabilities of HIV-1 and SIV proteases. *Biochemistry.* 31:9491–9501.

Griko, Y. V., P. L. Privalov, J. M. Sturtevant, and S. Y. Venyaminov. 1988. Cold denaturation of Staphylococcal nuclease. *Proc. Natl. Acad. Sci. USA.* 85:3343–3347.

Gryczynski, I., M. R. Eftink, and J. R. Lakowicz. 1988. Conformation heterogeneity in proteins as an origin of heterogeneous fluorescence decays, illustrated by native and denatured ribonuclease T_1. *Bichim. Biophys. Acta.* 954:244–252.

Hagerman, P. J., and R. L. Baldwin. 1976. Quantitative treatment of the kinetics of the folding transition of ribonuclease A. *Biochemistry.* 15: 1462–1473.

Hochstrasser, R. M., and D. K. Negus. 1984. Picosecond fluorescence decay of tryptophans in myoglobin. *Proc. Natl. Acad. Sci. USA.* 81:4399–4403.

Hynes, T. R., R. A. Kautz, M. A. Goodman, J. F. Gill, and R. O. Fox. 1989. Transfer of a β-turn structure to a new protein context. *Nature (Lond.).* 339:73–76.

James, E., P. G. Wu, W. Stites, L., and Brand. 1992. Compact denatured state of Staphylococcal nuclease mutant by guanidinium as determined by resonance energy transfer. *Biochemistry.* 31:10217–10225.

Jameson, D. M. 1984. Fluorescence: principles, methodologies, and applications. *In* Fluorescein Haptens: An Immunological Probe. E. Voss, Jr., editor. CRC Press, Boca Raton, FL. Chapter 3.

Johnson, M. L., and S. G. Fraiser. 1985. Non-linear least squares analysis. *Methods Enzymol.* 117:301–342.

Kirby, E. P., and R. F. Steiner. 1970. The influence of solvent and temperature upon the fluorescence of indole derivatives. *J. Phys. Chem.* 74: 4480–4490.

Knutson, J. R., L. Davenport, and L. Brand. 1986. Anisotropy decay associated fluorescence spectra and analysis of rotational heterogeneity. 1. Theory and applications. *Biochemistry.* 25:1805–1810.

Lakowicz, J. R. 1983. Principles of Fluorescence Spectroscopy. Plenum Press, New York.

Lakowicz, J. R., I. Gryczynski, H. Cheung, C-K. Wang, M. L. Johnson, and N. Joshi. 1988. Distance distributions in proteins recovered by using

frequency-domain fluorometry. Applications to troponin I and its complex with troponin C. *Biochemistry.* 27:9149–9160.

Lepock, J. R., K. P. Ritchie, M. C. Kolios, A. M. Rodahl, K. A. Heinz, and J. Kruuv. 1992. Influence of transition rates and scan rate on kinetic simulations of differential scanning calorimetry profiles of reversible and irreversible protein denaturation. *Biochemistry.* 31:12706–12712.

Lumry, R., R. Biltonen, and J. F. Brandts. 1966. Validity of the "two-state" hypothesis for conformational transitions in proteins. *Biopolymers.* 4:917–944.

Matthews, B. 1987. Genetic and structural analysis of the protein stability problem. *Biochemistry.* 26:6885–6888.

Mayorga, O. L., and E. Freire. 1987. Dynamic analysis of differential scanning calorimetry data. *Biophys. Chem.* 27:87–96.

Mei, G., N. Rosato, N. Silva, Jr., R. Rusch, E. Gratton, I. Savini, and A. Finazzi-Agro. 1992. Denaturation of human Cu/Zn superoxide dismutase by guanidine hydrochloride: A dynamnic fluorescence study. *Biochemistry.* 31:7224–7230.

Pace, C. N. 1986. Determination and analyis of urea and guanidine hydrochloride denaturation curves. *Methods Enzymol.* 131:266–280.

Pace, C. N., and G. R. Grimsley. 1988. Ribonuclease T_1 is stabilized by cation and anion binding. *Biochemistry.* 27:3242–3246.

Pace, C. N., D. V. Laurents, and J. A. Thomson. 1990. pH dependence of the urea and guanidine hydrochloride denaturation of ribonuclease A and ribonuclease T_1. *Biochemistry.* 29:2564–2572.

Pace, C. N., B. A. Shirley, and J. A. Thomson. 1989. Protein stability. *In* Protein Structure and Function: A Practical Approach. T. E. Creighton, editor. IRL Press, Oxford, England. 311–330.

Paladini, A. A., and G. Weber. 1981. Pressure-induced reversible dissociation of enolase. *Biochemistry.* 20:2587–2593.

Palleros, D. R., L. Shi, K. L. Reid, and A. L. Fink. 1993. Three-state denaturation of DnaK induced by guanidine hydrocholoride. Evidence for an expandable intermediate. *Biochemistry.* 32:4314–4321.

Parker, C. A. 1968. Photoluminescence of Solutions. Elsevier, London.

Petrich, J. W., M. C. Chang, D. B. McDonald, and G. R. Fleming. 1983. On the origin of nonexponential decay in tryptophan and its derivatives. *J. Am. Chem. Soc.* 105:3824–3832.

Privalov, P. L. 1989. Thermodynamic problems of protein structure. *Annu. Rev. Biophys. Biophys. Chem.* 18:47–69.

Privalov, P. L. 1990. Cold denaturation of proteins. *Crit. Rev. Biochem.* 25:281–305.

Ramsay, G. D., and M. R. Eftink. 1994. A multi-dimensional spectrophotometer for monitoring thermal unfolding transitions of macromolecules. *Biophys. J.* In press.

Royer, C. A., A. P. Hinck, S. N. Loh,, K. E. Prehoda, X. Peng, J. Jonas, and J. L. Markley. 1993. Effects of amino acid substitutions on the pressure denaturation of Staphylococcal nuclease A by fluorescence and nuclear magnetic resonance spectroscopy. *Biochemistry.* 32:5222–5231.

Royer, C. A., G. Weber, T. J. Daly, and K. S. Matthews. 1986. Dissociation of lactose repressor protein tetramer using high hydrostatic pressure. *Biochemistry.* 25:8308–8315.

Ross, J. B. A., H. R. Wyssbrod, R. A. Porter, G. P. Schwartz, C. A. Michaels, and W. R. Laws. 1992. Correlation of tryptophan fluorescence intensity decay parameters with ^{1}H NMR-determined rotamer conformations: [tryptophan^2]oxytocin. *Biochemistry.* 31:1585–1594.

Saito, Y., and A. Wada. 1983. Comparative study of GuHCl denaturation of globular proteins. I. Spectroscopic and chromatographic analysis of the denaturation curves of ribonuclease A, cytochrome *c*, and pepsinogen. *Biopolymers.* 22:2105–2122.

Santoro, M. M., and D. W. Bolen. 1988. Unfolding free energy changes determined by the linear extrapolation method. 1. Unfolding of phenylmethanesulfonyl α-chymotrypsin using different denaturants. *Biochemistry.* 27:8063–8068.

Schmid, F. X. 1989. Spectral methods of characterizing protein conformation and conformational changes. *In* Protein Structure. A Practical Approach. T. E. Creighton, editor. IRL Press, Oxford. 251–285.

Schellman, J. A. 1978. Solvent denaturation. *Biopolymers.* 17:1305–1322.

Schellman, J. A. 1987. The thermodynamic stability of proteins. *Annu. Rev. Biophys. Biophys. Chem.* 16:115–137.

Shortle, D., and A. K. Meeker. 1986. Mutant forms of Staphylococcal nuclease with altered patterns of guanidine hydrochloride and urea denaturation. *Proteins Struct. Funct. Genet.* 1:81–89.

Shortle, D., A. K. Meeker, and E. Freire. 1988. Stability mutants of Staphylococcal nuclease: Large compensating enthalpy-entropy changes for the reversible denaturation reaction. *Biochemistry.* 27:4761–4768.

Steiner, R. F. 1991. Fluorescence anisotropy: theory and applications. *In* Topics in Fluorescence Spectroscopy: Principles. Vol. 2. J. R. Lakowicz, editor. Plenum Press, New York. 1–52.

Straume, M., S. G. Fraiser-Cadoret, and M. L. Johnson. 1991. Least-squares analysis of fluroescence data. *In* Topics in Fluorescence Spectroscopy: Principles. Vol. 2. J. R. Lakowicz, editor. Plenum Press, New York. 177–240.

Sturtevant, J. M. 1987. Biochemical applications of differential calorimetry. *Annu. Rev. Phys. Chem.* 38:463–488.

Sugawara, T., K. Kuwajima, and S. Sugai. 1991. Folding of Staphylococccal nuclease A studied by equilibrium and kinetic circular dichroism spectra. *Biochemistry.* 30:2698–2706.

Szabo, A. G., and D. M. Rayner. 1980. Fluorescence decay of tryptophan conformers in aqueous solution. *J. Am. Chem. Soc.* 102:554–563.

Szabo, A. G., K. J. Willis, D. T. Krajcarski, and B. Alpert. 1989. Fluorescence decay parameters of tryptophan in a homogeneous preparation of human hemoglobin. *Chem. Phys. Lett.* 163:565–570.

Tanaka, A., J. Flanagan, and J. M. Sturtevant. 1993. Thermal unfolding of Staphylococcal nuclease and several mutant forms thereof studied by differential scanning calorimetry. *Protein Sci.* 2:567–576.

Thomson, J. A., B. A. Shirley, G. R. Grimsley, and C. N. Pace. 1989. Conformational stability and mechanism of folding of ribonuclease T_1. *J. Biol. Chem.* 264:11614–11620.

Timm, D. E., and K. E. Neet. 1992. Equilibrium denaturation studies of mouse β-nerve growth factor. *Protein Sci.* 1:236–244.

Vincent, M., J-C. Brochon, F. Merola, W. Jordi, and J. Gallay. 1988. Nanosecond dynamics of horse heart apocytochrome *c* in aqueous solution as studies by time-resolved fluroescence of the single tryptophan residue (Trp-59). *Biochemistry.* 27:8752–8761.

Weber, G., and H. G. Drickamer. 1983. The effect of high pressure upon proteins and other biomolecules. *Q. Rev. Biophys.* 16:89–112.

Zipp, A., and W. Kauzmann. 1973. Pressure denaturation of metmyoglobin. *Biochemistry.* 12:4217–4228.